NASA/TM—2006-214397

Modeling of Aerosols in Post-Combustor Flow Path and Sampling System

Thomas Wey
Taitech, Inc., Beavercreek, Ohio

Nan-Suey Liu
Glenn Research Center, Cleveland, Ohio

September 2006

NASA STI Program . . . in Profile

Since its founding, NASA has been dedicated to the advancement of aeronautics and space science. The NASA Scientific and Technical Information (STI) program plays a key part in helping NASA maintain this important role.

The NASA STI Program operates under the auspices of the Agency Chief Information Officer. It collects, organizes, provides for archiving, and disseminates NASA's STI. The NASA STI program provides access to the NASA Aeronautics and Space Database and its public interface, the NASA Technical Reports Server, thus providing one of the largest collections of aeronautical and space science STI in the world. Results are published in both non-NASA channels and by NASA in the NASA STI Report Series, which includes the following report types:

- TECHNICAL PUBLICATION. Reports of completed research or a major significant phase of research that present the results of NASA programs and include extensive data or theoretical analysis. Includes compilations of significant scientific and technical data and information deemed to be of continuing reference value. NASA counterpart of peer-reviewed formal professional papers but has less stringent limitations on manuscript length and extent of graphic presentations.

- TECHNICAL MEMORANDUM. Scientific and technical findings that are preliminary or of specialized interest, e.g., quick release reports, working papers, and bibliographies that contain minimal annotation. Does not contain extensive analysis.

- CONTRACTOR REPORT. Scientific and technical findings by NASA-sponsored contractors and grantees.

- CONFERENCE PUBLICATION. Collected papers from scientific and technical conferences, symposia, seminars, or other meetings sponsored or cosponsored by NASA.

- SPECIAL PUBLICATION. Scientific, technical, or historical information from NASA programs, projects, and missions, often concerned with subjects having substantial public interest.

- TECHNICAL TRANSLATION. English-language translations of foreign scientific and technical material pertinent to NASA's mission.

Specialized services also include creating custom thesauri, building customized databases, organizing and publishing research results.

For more information about the NASA STI program, see the following:

- Access the NASA STI program home page at *http://www.sti.nasa.gov*

- E-mail your question via the Internet to *help@sti.nasa.gov*

- Fax your question to the NASA STI Help Desk at 301–621–0134

- Telephone the NASA STI Help Desk at 301–621–0390

- Write to:
  NASA STI Help Desk
  NASA Center for AeroSpace Information
  7121 Standard Drive
  Hanover, MD 21076–1320

NASA/TM—2006-214397

Modeling of Aerosols in Post-Combustor Flow Path and Sampling System

Thomas Wey
Taitech, Inc., Beavercreek, Ohio

Nan-Suey Liu
Glenn Research Center, Cleveland, Ohio

National Aeronautics and
Space Administration

Glenn Research Center
Cleveland, Ohio 44135

September 2006

Acknowledgments

Many thanks go to Ian Waitz of the Massachusetts Institute of Technology, Richard Miake-Lye of Aerodyne Research, Inc., and Chowen Wey of the NASA Glenn Research Center for their thoughtful interactions with us. We also would like to thank Robert Howard and Robert Hiers of the Air Force Arnold Engineering Development Center for providing the geometry of the dilution probes.

This work was sponsored by the Fundamental Aeronautics Program at the NASA Glenn Research Center.

Level of Review: This material has been technically reviewed by technical management.

Available from

NASA Center for Aerospace Information
7121 Standard Drive
Hanover, MD 21076–1320

National Technical Information Service
5285 Port Royal Road
Springfield, VA 22161

Available electronically at http://gltrs.grc.nasa.gov

Modeling of Aerosols in Post-Combustor Flow Path and Sampling System

Thomas Wey
Taitech, Inc.
Beavercreek, Ohio 45430

Nan-Suey Liu
National Aeronautics and Space Administration
Glenn Research Center
Cleveland, Ohio 44135

Abstract

The development and application of a multi-dimensional capability for modeling and simulation of aviation-sourced particle emissions and their precursors are elucidated. Current focus is on the role of the flow and thermal environments. The cases investigated include a film cooled turbine blade, the first-stage of a high-pressure turbine, the sampling probes, the sampling lines, and a pressure reduction chamber.

1. Introduction

Aircraft emissions can influence the climate change of the atmosphere and health responses in the vicinity of the airports. To alleviate these increasingly significant impacts on the environment, it is necessary to acquire a better understanding of the formation and subsequent development of gaseous pollutants, aerosols (volatile particles and soot) and their precursors in the internal flow and in the plume of the jet engines operating over the full range from ground to flight altitude. This could be achieved through efforts which combine the use of accurate measurement and high-fidelity modeling and simulation.

The volatile nature of the aerosols introduces difficulties in their repeatable and accurate measurement because their concentration and size can be quite sensitive to the sampling conditions and procedures. These difficulties are sometimes further compounded by the necessity of in-situ measurements, i.e., sampling from aircraft in flight. Clearly, the ability to predict the effects of sampling conditions and procedures on the aerosol behavior will greatly assist the development of sampling techniques and the optimization of sampling procedures for making accurate and quantitative measurements of particulate emissions.

Current modeling studies often have used low-order methods, where chemical kinetics and/or particle microphysics are driven by averaged flow parameters specified as a function of time (e.g. [1], [2], [3], [4]). In some flow regions and for certain chemical or microphysical processes, these low-order methods could adequately capture the overall activities. Nevertheless, the more complex multi-dimensional analysis needs be applied to flow regions in which the chemical or the microphysical activities could be appreciably influenced by flow non-uniformity, particularly in thermodynamic conditions and residence time.

This paper describes a Computational Fluid Dynamics (CFD) based modeling and simulation tool for complementing limited measurement studies and addressing the sampling system issues. It accounts for and integrates fluid dynamics, chemistry and particle microphysics relevant to aircraft emissions. The discussion proceeds as follows. Section 2 presents the conservation equations for the gas-phase flow. Section 3 describes the continuity equation for aerosol transport. Section 4 discusses the implemented models of various microphysical processes such as thermophoresis, coagulation, nucleation, soot activation, condensation, and the interaction between the gaseous species and the particles. Section 5 presents the application of this multi-dimensional modeling and simulation tool. The cases investigated include a film cooled turbine blade, the first-stage of a high-pressure turbine, the sampling probes, the sampling lines, and a pressure reduction chamber. Section 6 summarizes the current state of the progress and suggests areas warranting future improvements.

2. Governing Equations for Gas-phase Flow

The conservation equations for the gas-phase flow in the multiple rotating frames of reference (MRF) which is convenient for including the rotational components of the jet engine in the computational domain are summarized in a hybrid formulation below.
Continuity equation:

$$\frac{d}{dt}\iiint_V \rho\, dV + \iint_A \rho(\vec{u} - \vec{U}_g)\cdot d\vec{A} = 0 \tag{1}$$

Species transport equation:

$$\frac{d}{dt}\iiint_V \rho_m\, dV + \iint_A \rho_m(\vec{u} - \vec{U}_g)\cdot d\vec{A} = \iint_A \rho D_{eff}\nabla\left(\frac{\rho_m}{\rho}\right)\cdot d\vec{A} + \iiint_V \dot{w}_m'''\, dV \tag{2}$$

Momentum equation:

$$\frac{d}{dt}\iiint_V \rho\vec{u}\, dV + \iint_A \rho\vec{u}(\vec{u} - \vec{U}_g)\cdot d\vec{A} = -\iint_A p\, d\vec{A} + \iint_A \tau\cdot d\vec{A} - \iiint_V \rho\vec{\omega}_g \times \vec{u}\, dV \tag{3}$$

Energy equation:

$$\frac{d}{dt}\iiint_V \rho E\, dV + \iint_A \rho E(\vec{u} - \vec{U}_g)\cdot d\vec{A} = -\iint_A p\vec{u}\cdot d\vec{A} - \iint_A \vec{q}\cdot d\vec{A} + \iint_A \vec{u}\cdot\tau\cdot d\vec{A} \tag{4}$$

Turbulence equations:

$$\frac{d}{dt}\iiint_V \rho k\, dV + \iint_A \rho k(\vec{u} - \vec{U}_g)\cdot d\vec{A} = S_k + \iint_A \left(\mu + \frac{\mu_t}{\sigma_k}\right)\nabla k\cdot d\vec{A} \tag{5}$$

$$\frac{d}{dt}\iiint_V \rho\varepsilon\, dV + \iint_A \rho\varepsilon(\vec{u}-\vec{U}_g)\cdot d\vec{A} = S_\varepsilon + \iint_A (\mu + \frac{\mu_t}{\sigma_\varepsilon})\nabla\varepsilon \cdot d\vec{A} \qquad (6)$$

where

$$\vec{q} = -\kappa\nabla T,$$

$$\tau = -\frac{2}{3}\mu(\nabla\cdot\vec{u})\mathbf{I} + \frac{1}{2}\mu(\nabla\vec{\mathbf{u}} + (\nabla\vec{\mathbf{u}})^{\mathbf{T}}),$$

V is an arbitrary control volume with control surface A, ρ is the fluid density, ρ_m is the partial density of species m, $\dot{w}_m^{'''}$ is the production rate of species m per unit volume, $\vec{u}$ is the flow velocity in a stationary Cartesian coordinate system, $\vec{\omega}_g$ is the grid rotating velocity for each designated axis, $\vec{U}_g = \vec{\omega}_g \times \vec{r}$, E is the total energy density, k is the turbulent kinetic energy, ε is the turbulent dissipation rate, S_k is the source term for k, S_ε is the source term for ε, p is the static pressure, τ is the viscous stress tensor, $\vec{q}$ is the heat flux vector, D_{eff} is the effective mass diffusivity coefficient which is equal to $\frac{\mu_t+\mu}{\rho Sc}$, κ, μ and μ_t are the thermal conductivity, laminar viscosity and turbulent viscosity, respectively. For gas, the Schmidt number (Sc) is about 1. Different angular velocities (and even different rotating axes) are assigned to different mesh blocks or groups within the model. Balance equations for each group are expressed in the relative reference frame but in terms of the absolute velocity (i.e. the velocity with respect to a stationary coordinate system).

3. General Dynamic Equation

A general dynamic equation (GDE) is the continuity equation for aerosol transport. Because the GDE is a nonlinear, partial integro-differential equation, analytical solutions are available for only a few special cases [5, 6]. Aerosols are often described in terms of size distributions, i.e. the number of particles in a given size bin. Therefore a multiple size bin model is adopted here to approximate the aerosol general dynamic equations (GDE). Since the governing equations for gas-phase flow are written in the multiple rotating frames of reference (MRF), the GDE will be cast in this reference system too. Furthermore, it is written in a discrete form as a population balance for each cluster or particle size, and it describes particle dynamics under the influence of various physical phenomena: convection, diffusion, coagulation, nucleation, condensation, evaporation and external force field.

$$\frac{d}{dt}\iiint_V N_k\, dV + \iint_A N_k(\vec{u}-\vec{U}_g)\cdot d\vec{A} = \iint_A (D_M + \frac{2\nu_t}{3\sqrt{C_u f_u}})\nabla N_k \cdot d\vec{A}$$
$$+\iiint_V \left.\frac{dN_k}{dt}\right|_{micro} dV,$$
$$k = 1,\cdots, M_B \qquad (7)$$

where N_k is the number density of particles in size bin k, M_B is the total number of

the size bins, $\vec{u}$ is the flow velocity in a stationary Cartesian coordinate system,[1] ν_t is turbulent kinematic viscosity, C_u is 0.09, f_u is the damping function of the turbulence model. The effective molecular (Brownian) diffusivity coefficient, D_M, is defined as

$$D_M = \frac{k_B T C c_k}{3\pi\mu_g d_{p,k}}, \tag{8}$$

All the variables in the above equation will be defined in the following sections. $\left.\frac{dN_k}{dt}\right|_{micro}$ represents the summation of microphysical processes,

$$\left.\frac{dN_k}{dt}\right|_{micro} = \left.\frac{dN_k}{dt}\right|_{drifting} + \left.\frac{dN_k}{dt}\right|_{coagulation} + \left.\frac{dN_k}{dt}\right|_{nucleation} + \left.\frac{dN_k}{dt}\right|_{cond./evap.} \tag{9}$$

The first term in Equation (9) is associated with the drifting velocity caused by external forces, e.g., the thermophoretic force, the lift-drag force, the electrophoresis and gravitational force. As for the rest of the terms, coagulation means that the particles collide and attach to each other; nucleation represents the formation of the nuclei of new particles; and condensation indicates that molecular mass transfer from the vapor phase to the particles, while evaporation is the reverse process of the condensation. In the present work, the particle number density on a solid wall is assumed to be zero or a fraction of the value at a point next to a solid wall.

4. Models for Particle Microphysical Processes

The most important and efficient binary nucleation in the atmosphere is that of sulfuric acid and water. A free sulfuric acid molecule tends to gather water molecules around it to form hydrates. The main reason is that H_2SO_4 has extremely low saturation vapor pressure. Doyle [7] showed that even when relative humidity is less than 100%, extremely small amount of H_2SO_4 vapor are able to induce nucleation. Within the turbine engine exhaust, major gas-phase chemical reactions will take place, and soot activation [8, 9] into water condensation nuclei also occurs. If the surface of a foreign particle (e.g., soot) does participate in the gas-to-particle conversion process, the nucleation is referred to as heterogeneous. More detailed discussions on soot activation and condensation of water and sulfuric acid can be found in Wang's work [9]. The first elemental step in heterogeneous nucleation involves molecular adsorption which is between soot and H_2SO_4 and SO_3. The nano-size aerosols will collide with each other and stick together. Such a process is the called coagulation and it will change the particle size distributions.

4.1. Characteristics of Particles

In the present work, we assume that

- All particles are assumed to be spherical.
- Heat and momentum transfer between the carrier gas and the particles is negligible.
- Gas turbulence influences the particles, but the particles do not influence the gas turbulence.

[1]For noninertial particles (i.e. extremely small aerosols) advected by a turbulent flow, particle velocity coincides with carrier velocity. In the present work, all particles are treated as noninertial for simplicity.

- No particle is charged.
- The particle size distribution of soot entering the post-combustor region is always prescribed.
- All particles are noninertial.

Based upon the sectional approach, the total volume range for the particles is divided into M_B bins. Using a geometric progressing factor, the volume of a particle in each bin can be calculated easily. For example, in an aerosol system, the particle size ranges from 1 nm to about 1 μm, hence, the corresponding volume ranges from $10^{-27} m^3$ to $10^{-18} m^3$. To cover the 9 orders of magnitude volume span with 12 bins, the bins are linearly spaced on a logarithmic scale, so that $\upsilon_k = 10^{9/(12-1)} \upsilon_{k-1}$, where υ_k is the volume of a particle in size bin k.

4.2. Thermophoresis

Thermophoresis arises from the temperature gradients in the carrier gas: small particles drift from hot regions towards cold regions. Brock [10] derived the following expression for the thermophoretic velocity, $\vec{V}_{TH_k}$

$$\vec{V}_{TH_k} = \frac{-3Cc_k(k_g + c_t k_p Kn_k)}{(1+3c_m Kn_k)(k_p + 2k_g + 2c_t k_p Kn_k)} \left[\frac{\mu_g}{\rho_g T} \right] \nabla T \tag{10}$$

where μ_g is the viscosity of the carrier gas, k_g and k_p are the gas and particle thermal conductivities, respectively, and c_m and c_t are phenomenological coefficients known as the "isothermal slip" coefficient and the "temperature jump" coefficient, representative values according to Brock [10] are $c_t = 2.2$ and $c_m = 1.0$ .The smaller the diameter of a particle, the larger the effect of the thermophoretic force. Since the turbulent thermal diffusion discussed by Elperin [11] is not included in the present model, we have

$$\left. \frac{dN_k}{dt} \right|_{drifting} = -\nabla \cdot (\vec{V}_{TH_k} N_k) \tag{11}$$

When the Knudsen number is much larger than one, i.e., $Kn_k \gg 1$ (particles are much smaller than the mean free path of the carrier gas), an alternative form for the laminar thermophoretic velocity is given by [12]:

$$\vec{V}_{TH_k} = \frac{-3}{4(1+\pi\alpha/8)} \left[\frac{\mu_g}{\rho_g T} \right] \nabla T \qquad (Kn_k \gg 1) \tag{12}$$

where the negative sign indicates that the motion is in the direction of decreasing temperature, and α is the nondimensional thermal accommodation coefficient, its typical value is about 0.9. The thermophoretic velocity for $Kn_k \gg 1$ is independent of the particle size. Furthermore, it is nearly independent of the particle material.

4.3. Coagulation

Aerosol coagulation is important because it changes the size distribution and the composition of particles. Coagulation is a process where particles in a population

collide with each other and stick together to form larger particles [13]. The total volume is conserved in a coagulating aerosol ensemble. Collisions between aerosols can be initiated by gravitational settling, turbulence, and thermal (Brownian) motion. For particles smaller than one micrometer in diameter, the most important collision process is the Brownian motion, which is considered in the current work. Different approaches have been developed in the past to simulate coagulation, depending upon the need and availability of computer resources. Since the model has to be incorporated into a three-dimensional CFD program, a semi-implicit scheme [14] is adopted here. All the particles are assumed to be spherical. Soot density is less than that of carbon black and usually in the range of 1700-1800 kg/m^3 depending on the porosity of soot. Soot particles are generally small, ranging in size from 5 nm to 90nm, but may be up to several micrometers in extreme cases. Soot scavenging by coagulation occurs when a small H_2SO_4-H_2O droplet collides with a larger coated soot.

4.3.1. Single particle size distribution

The rate of change of a single particle size distribution (PSD) due to coagulation is given by a modified Smoluchowski Equation,

$$\left.\frac{dN_k}{dt}\right|_{coag} = \frac{1}{2}\sum_{j=1}^{k-1} B_{j,k-j} N_{k-j,t} N_{j,t} - N_{k,t}\sum_{j=1}^{\infty} B_{k,j} N_{j,t} \tag{13}$$

where $B_{k,j}$ ($m^3/(s\ particle)$) is the coagulation kernel or collision frequency function of two colliding particles. A volume-conserving solution [15] is given by

$$\upsilon_k N_{k,t} = \frac{\upsilon_k N_{k,t-h} + h\sum_{j=1}^{k}\left(\sum_{i=1}^{k-1} f_{i,j,k} B_{i,j} \upsilon_i N_{i,t} N_{j,t-h}\right)}{1 + h\sum_{j=1}^{M_B}\left(1 - f_{k,j,k}\right) B_{k,j} N_{j,t-h}} \tag{14}$$

where υ_k is the volume of a particle in size bin k, M_B is the total number of bins, h is the CFD time step used in the solution of the carrier gas. When two particles collide and stick together, the volume of the intermediate particle is

$$V_{i,j} = \upsilon_i + \upsilon_j \tag{15}$$

If this volume falls between two bins, the new particle is split into adjacent bins as follows.

$$f_{i,j,k} = \begin{cases} \left[\dfrac{\upsilon_{k+1} - V_{i,j}}{\upsilon_{k+1} - \upsilon_k}\right]\dfrac{\upsilon_k}{V_{i,j}} & \upsilon_k \le V_{i,j} < \upsilon_{k+1} \quad k<M_B \\ 1 - f_{i,j,k-1} & \upsilon_{k-1} < V_{i,j} < \upsilon_k \quad k>1 \\ 1 & V_{i,j} \ge \upsilon_k \quad k=M_B \\ 0 & all\ other\ cases \end{cases} \tag{16}$$

The generalized Brownian coagulation kernel $B_{i,j}$ for collision of particles of volume υ_i and υ_j is given by Fuchs [13]

$$B_{i,j} = \frac{2\pi(d_i + d_j)(D_{p,i} + D_{p,j})}{\dfrac{d_i + d_j}{d_i + d_j + (\delta_i^2 + \delta_j^2)^{1/2}} + \dfrac{8(D_{p,i} + D_{p,j})}{(d_i + d_j)(\bar{c}_{p,i}^2 + \bar{c}_{p,j}^2)^{1/2}}} \tag{17}$$

where d_i and d_j are the diameters of particles in the i th and j th size bins, the unit of $B_{i,j}$ is $m^3/(s\ particle)$, $D_{p,i}$ or $D_{p,j}$ is the particle diffusion coefficient in the i th or j th size bins and is given by

$$D_{p,i} = \frac{k_B T C c_i}{3\pi d_{p,i} \mu_g} \tag{18}$$

where k_B is the Boltzmann constant (= $1.380658 \times 10^{-23} JK^{-1} molec.^{-1}$), T is the absolute temperature (K), $d_{p,i}$ is the diameter of the size-i particle, and μ_g is the dynamic viscosity of the carrier gas. The Cunningham-slip factor is defined as

$$Cc_i = 1 + Kn_i(1.257 + 0.4e^{-1.1/Kn_i}) \tag{19}$$

where Kn_i is the Knudsen number defined as the ratio of the mean free path of the carrier gas, λ_g, to the diameter of the size-i particle

$$Kn_i = \frac{2\lambda_g}{d_{p,i}} \tag{20}$$

The mean free path of the carrier gas depends upon the pressure, temperature, molecular weight of the carrier gas, and the universal gas constant, it is given by

$$\lambda_g = \frac{2\mu}{p_g\left(\frac{8\overline{MW}_g}{\pi R_u T}\right)^{1/2}} \tag{21}$$

$\overline{c}_{p,i}$ is the mean thermal speed of a particle in size bin i,

$$\overline{c}_{p,i} = \left(\frac{8k_B T}{\pi m_i}\right)^{1/2} \tag{22}$$

where m_i is the mass of a particle in size bin i. δ_i is a correction factor which represents the mean distance between the center of a sphere and a particle which has bounced from the surface of the sphere and has traveled a distance of one particle mean free path, it is given by

$$\delta_i = \frac{(d_{p,i} + \lambda_{p,i})^3 - (d_{p,i}^2 + \lambda_{p,i}^2)^{3/2}}{3 d_{p,i} \lambda_{p,i}} - d_{p,i} \tag{23}$$

The particle mean free path of a particle in size bin i is

$$\lambda_{p,i} = \frac{8D_{p,i}}{\pi \overline{c}_{p,i}} \tag{24}$$

Finally, the change of the size distribution due to coagulation is

$$\left.\frac{dN_k}{dt}\right|_{coag} = \frac{N_{k,t} - N_{k,t-h}}{h} \tag{25}$$

4.3.2. Multiple particle size distributions

Coagulation among multiple particle distributions (e.g. among the soot particles and the H_2SO_4-H_2O liquid droplets) is also considered in the current study. Coagulation among

two independent size distributions will add one more particle size distribution for the resultant particle, hence, the total number of particle size distributions becomes three. Here, the semi-implicit coagulation solution is extended to treat coagulation involving three different size distributions (e.g. $N_T = 3$), with size bins in each distribution being M_B. The resultant particle number density of the Y distribution in bin k at time t during coagulation is defined as

$$N_{Yk,t} = \frac{N_{Yk,t-h} + h(T_1 + T_2)}{1 + hT_3}, \tag{26}$$

where

$$T_1 = \frac{1}{\upsilon_{Yk}} \sum_{M=1}^{N_T} \left[P_{Y,M} \sum_{j=1}^{k} \left(N_{Mj,t-h} \sum_{i=1}^{k-1} f_{Yi,Mj,Yk} B_{Yi,Mj} \upsilon_{Yi} N_{Yi,t} \right) \right], \tag{27}$$

$$T_2 = \frac{1}{\upsilon_{Yk}} \sum_{M=1}^{N_T} \sum_{I=1}^{N_T} \left[Q_{I,M,Y} \sum_{j=1}^{k} \left(N_{Mj,t-h} \sum_{i=1}^{k} f_{Ii,Mj,Yk} B_{Ii,Mj} \upsilon_{Ii} N_{Ii,t} \right) \right], \tag{28}$$

$$T_3 = \sum_{j=1}^{M_B} \left[\sum_{M=1}^{N_T} [(1 - L_{Y,M})(1 - f_{Yk,Mj,Yk}) + L_{Y,M}] B_{Yk,Mj} N_{Mj,t-h} \right], \tag{29}$$

Term T_1 accounts for the production of larger particles in distribution Y from self-coagulation and from heterocoagulation between distribution Y and distribution $M \neq Y$. Term T_2 accounts for the production of particles in distribution Y from heterocoagulation among the other two independent distributions ($I \neq Y$ and $M \neq Y$). The first part of term T_3 accounts for self-coagulation loss in distribution Y to larger sizes, while the second part accounts for loss of distribution Y to all other distributions due to heterocoagulation between the Y distribution and the other distributions.

If the volume of the new particle falls between two bins, it is split into adjacent bins as follows.

$$f_{Ii,Mj,Yk} = \begin{cases} \left[\dfrac{\upsilon_{Yk+1} - V_{Ii,Mj}}{\upsilon_{Yk+1} - \upsilon_{Yk}} \right] \dfrac{\upsilon_{Yk}}{V_{Ii,Mj}} & \upsilon_{Yk} \le V_{Ii,Mj} < \upsilon_{Yk+1} \quad k < M_B \\ 1 - f_{Ii,Mj,Yk-1} & \upsilon_{Yk-1} < V_{Ii,Mj} < \upsilon_{Yk} \quad k > 1 \\ 1 & V_{Ii,Mj} \ge \upsilon_k \quad k = M_B \\ 0 & \textit{all other cases} \end{cases} \tag{30}$$

The values of P, Q, and L in equations (27-29) are either 1 or 0, depending on the specifics of the coagulation considered. Parameter $P_{Y,M} = 1$, if the coagulation between particles in distribution Y and in distribution M produces larger particles in distribution Y. For example, $P_{soot,soot} = 1$, and $P_{H_2SO_4 - H_2O, H_2SO_4 - H_2O} = 1$. Parameter $Q_{I,M,Y} = 1$, if the coagulation between particles in distribution I and in distribution M

produces particles in distribution Y, where $I \neq M$ and $I \neq Y$. For example, $Q_{soot,H_2SO_4-H_2O,mix} = 1$, and $Q_{H_2SO_4-H_2O,soot,mix} = 1$. Parameter $L_{Y,M} = 1$, if the coagulation between particles in distribution Y and in distribution M *does not* produce particles in distribution Y. For example, $L_{soot,H_2SO_4-H_2O} = 1$, and $L_{H_2SO_4-H_2O,soot} = 1$.

Finally, the change of the size distribution for each type of aerosol due to coagulation is

$$\left.\frac{dN_{Yk}}{dt}\right|_{coag} = \frac{N_{Yk,t} - N_{Yk,t-h}}{h} \tag{31}$$

4.4. Homogeneous Binary Nucleation of H_2SO_4-H_2O

The classical nucleation theory assumes that as the state of current phase is becoming unstable, a new phase is formed. It is based on the equilibrium state of small liquid drops, or embryos, in contact with their parent vapors; some of the embryos, which become freely growing droplets, are said to be "nucleated". The theory predicts the nucleation rate as follows:

$$J_{hom} = \pi d^{*2} \beta_{H_2SO_4} N_{H_2O} \exp\left(-\frac{\Delta G^*}{R_u T}\right) \tag{32}$$

where J_{hom} is the homogeneous nucleation rate ($particle/(m^3 s)$), $\pi d^{*2} \beta_{H_2SO_4} N_{H_2O}$ is a prefactor term, ΔG^* is the change of the Gibbs free energy (J/mol) during the phase change, R_u is the universal gas constant. The change of the Gibbs free energy is a function of the number of sulfuric acid and water molecules and is represented by a two dimensional energy surface. To become stable, a cluster will have to follow the path of least energy on this surface, thus leading to the so-called saddle point. To avoid solving iteratively to find the roots of the equations which satisfy the saddle point condition, the parameterization of Kulmala et al. [16], updated by Vehkamäki et al. [17] for low temperature emissions and by Vehkamäki et al. [18] for high temperature emissions, is used here (See Appendix A). This scheme provides the nucleation rate $J_{H_2SO_4-H_2O}$ (number of new embryos formed per second and per cubic meter) in the water/sulfuric acid mixture, and the critical cluster composition (total number of molecules and sulfuric acid mole fraction). These parameterized equations reduce the computing time by a factor of 500 compared to non-parameterized nucleation rate calculations.

4.4.1. Low Temperature Range

The parameterized formulas are valid for temperatures between 190.15 K and 305.15 K, relative humidity between 0.01% and 100%, and total sulfuric acid molecule number from 10^{10} to 10^{17} m^{-3}. The parameterization is limited to cases where nucleation rates are between 10^{-1} and 10^{16} $m^{-3}s^{-1}$ and the critical cluster contains at least four molecules. For the cases where the temperature is below190.15 K, a zeroth order extrapolation is applied to the nucleation rate. More details can be found in Appendix A.

4.4.2. High Temperature Range

The parameterized formulas are valid for temperature between 300.15 K and 400.15 K, relative humidity between 1% and 100%, and total sulfuric acid molecule number from 2×10^{15} to 5×10^{21} *molecule* m^{-3}. The parameterization is limited to cases where nucleation rates are between 10^{5} and 10^{20} *particle* $m^{-3}s^{-1}$ and the critical cluster contains at least four molecules. For the cases where the temperature is above 400.15 K, a zeroth order extrapolation is applied to the nucleation rate. More details can be found in Appendix A. It is noted here that, for sulfuric acid solution, experimental data are available for its surface tension when $T < 323K$, for its density when $T < 373K$, and for its *activities*[2] when $T < 350K$. The computed nucleation rates and other thermodynamic properties may be of greater uncertainty when the temperature is out of the experimental range.

4.5. Soot Activation

Since soot is hydrophobic, it must be activated in order to be capable of taking up water from the gas phase. Soot can be activated as water condensation nuclei by adsorption[3] of oxidized sulfur species (H_2SO_4 and SO_3) and by scavenging, i.e., coagulation with volatile sulfate aerosols.

The fraction of soot surface due to the above two activation pathways is $\theta_i = \theta_{ads,i} + \theta_{sca,i}$, where i is the index of the size bin. Kärcher [8] presented a kinetic formula for $\theta_{ads,i}$:

$$\frac{d\theta_{ads,i}}{dt} = .25\alpha\bar{c}(C_{SO_3} + C_{H_2SO_4})\times 6.02\times10^{23}\frac{1-\theta_i}{\sigma_0} \tag{33}$$

where α is the sticking probability. It is either set to zero for $T > 420K$ or set to unity for $T \le 420\ K$. $\bar{c}$ is the mean thermal speed for SO_3, C is the molar density of gas phase species, (mol/m^3), and σ_0 is the average number of sites per unit area of soot surface ($\sigma_0 \approx 5\times10^{18} m^{-2}$). This formula which assumes that the vapor adsorption on fresh soot takes place in the gas kinetic regime gives the maximum adsorbed sulfur mass, and it represents the upper bound of the binary H_2SO_4-H_2O heterogeneous nucleation rate on the soot surface.

The change of surface coverage for a soot particle in size bin i by scavenging volatile (H_2SO_4-H_2O) droplets from size bin $j = 1$ to $j = M_B$ is determined by

$$\frac{d\theta_{sca,i}}{dt} = .25\pi\times\sum_{j=1}^{M_B} B_{i,j}N_j d_{p,j}^2 \times\frac{1-\theta_i}{d_{p,i}^2} \tag{34}$$

where $B_{i,j}$ is the coagulation kernel between soot in size bin i and H_2SO_4-H_2O in size

[2]The product of the mole fraction of a solution component and its activity coefficient is defined as the activity of the component.

[3]When a gas is brought into contact with a solid particle and part of it is taken up by the solid surface, the process is known as adsorption. If the interactions between the gas and the solid are weak, such as between sulfur species and soot, the process is called physical adsorption which is characterized by the molecular bonding.

bin j, N_j is the number density of H_2SO_4-H_2O in size bin j, $d_{p,j}^2$ is the diameter of H_2SO_4-H_2O droplets in size bin j, and $d_{p,i}^2$ is the diameter of soot in size bin i.

The gas phase depletion of H_2SO_4 and SO_3 due to adsorption is proportional to $(1-\theta_i)$, i.e., the available "dry" soot surface area, they are determined from as follows.

$$\left.\frac{dC_{SO_3}}{dt}\right|_{ads} = -.25\alpha\bar{c}C_{SO_3}\sum_{i=1}^{M_B} N_i d_{p,i}^2(1-\theta_i) \tag{35}$$

$$\left.\frac{dC_{H_2SO_4}}{dt}\right|_{ads} = -.25\alpha\bar{c}C_{H_2SO_4}\sum_{i=1}^{M_B} N_i d_{p,i}^2(1-\theta_i) \tag{36}$$

where N_i is the number density of soot in size bin i. This model also accounts for the condensation of H_2SO_4-H_2O on the "wetted" soot surface area. Consequently, condensation rates onto soot particles and corresponding gas phase depletion of H_2SO_4 and H_2O are proportional to θ_i.

Finally, using a semi-implicit method, θ_i is evaluated by

$$\theta_i^t = \frac{\theta_i^{t-h} + h(Q_{ads} + Q_{sca})}{1 + h(Q_{ads} + Q_{sca})} \tag{37}$$

where

$$Q_{ads} = .25\frac{\alpha}{\sigma_0}\bar{c}(C_{SO_3} + C_{H_2SO_4}) \times 6.02 \times 10^{23} \tag{38}$$

and

$$Q_{sca} = .25\frac{\pi}{d_{p,i}^2} \times \sum_{j=1}^{M_B} B_{i,j} N_j d_{p,j}^2 \tag{39}$$

4.6. Condensation of Water and Sulfuric Acid

If the vapor pressure of H_2SO_4 or H_2O is in excess of the equilibrium vapor pressure, condensation will occur. Condensation can occur on the liquid H_2SO_4-H_2O aerosols as well as on the liquid coating of soot surface. If the vapor pressure of H_2SO_4 is less than the equilibrium vapor pressure, then the sulfuric acid molecules will evaporate from the H_2SO_4-H_2O aerosols. However, the equilibrium vapor pressure of H_2SO_4 over the liquid droplets is so small that, once H_2SO_4 molecules are condensed, they can hardly re-evaporate. In contrast, H_2O will condense to and evaporate from the droplets depending on the evolution of temperature and the partial pressure of H_2O in the carrier gas.

Following Fukuta and Walter [9, 19], the condensational growth of $m = H_2O$, or H_2SO_4 onto particles in the size bin k is given by:

$$\frac{dn_{m,k}}{dt} = 4\pi r_k D_{v,m,k}^* \left(\frac{p_m - p_{m,k,sat}}{R_u T}\right) \tag{40}$$

where $\frac{dn_{m,k}}{dt}$ is the rate of change in moles of species m due to condensation onto or evaporation from an aerosol with radius r_k, the modified diffusivity is

$$D^*_{v,m,k} = \frac{D_{v,m}}{\frac{r_k}{r_k + \lambda_g} + \frac{4D_{v,m}}{r_k \bar{c}_m}} \tag{41}$$

where λ_g is defined in Equation (21), $D_{v,m}$ is the diffusivity of species m, as defined in Appendix B.

The mean thermal velocity of gaseous species m is given by

$$\bar{c}_m = \left(\frac{8R_u T}{\pi \overline{MW}_m} \right)^{1/2} \tag{42}$$

It should be noted here that, when calculating the condensation on soot particles, since only the activated surface of soot can accept the diffusion of the molecules of H_2SO_4 and H_2O, the right hand side of equation (40) needs to be multiplied by the fraction θ_k provided via equation (37).

The saturation vapor pressure is computed from Kelvin equation which implies that the curvature will increase the value of the saturation vapor pressure of species m,

$$\frac{p_{m,k,sat}}{p^{flat}_{m,sat}} = \exp\left(\frac{2\sigma \bar{v}_m}{R_u T r_k} \right) \tag{43}$$

where σ is the surface tension of a liquid droplet ($Joule/m^2$), $\bar{v}_m$ is the partial molar volume of species m in a solution (m^3/mol), $p_{m,k,sat}$ is the saturation vapor (partial) pressure of gaseous species m over a spherical droplet of radius r_k, and $p^{flat}_{m,sat}$ is the saturation vapor (partial) pressure of species m over a flat liquid surface with the same composition as the droplet. The effect of curvature is important for droplets smaller than 0.1 μm. Further details of various thermodynamic properties of aerosols are given in Appendix B.

Now, let dr_k/dt be the radial growth rate of a particle (volatile droplet or soot coated with H_2SO_4-H_2O) in size bin k due to condensation and $V_{cond} = \upsilon_k + 4\pi r_k^2 \frac{dr_k}{dt} h$ be the new particle volume, the rate of change of particle size due to condensation ($V_{cond} > \upsilon_k$) and evaporation ($V_{cond} < \upsilon_k$) per unit time and per cubic meter of carrier gas can be expressed as

$$G_k = \left(\sum_{j=1}^{M_B} f_{c,j,k} N_j - N_k \right) / h \tag{44}$$

where $f_{c,k,j}$, a modified volume splitting operator, is defined as

$$f_{c,k,j}=\begin{cases}\left[\dfrac{\upsilon_{j+1}-V_{cond}}{\upsilon_{j+1}-\upsilon_j}\right] & \upsilon_j \le V_{cond} < \upsilon_{j+1} \quad j<M_B \\ 1-f_{c,k,j-1} & \upsilon_{j-1}<V_{cond}<\upsilon_j \quad j>1 \\ 1 & V_{cond} \ge \upsilon_j \quad j=M_B \\ \dfrac{V_{cond}}{\upsilon_1} & V_{cond} < \upsilon_1 \quad j=1 \end{cases} \tag{45}$$

The first term on the right hand side of equation (44) represents the production of particles in size bin k due to condensation and evaporation. The last term is the destruction of particles in size bin k by condensation and evaporation. $(dN_k/dt)_{cond./evap.}$ is expressed as

$$\left(\frac{dN_k}{dt}\right)_{cond./evap.} = G_k \tag{46}$$

The change of radius due to condensation or evaporation is

$$\frac{dr_k}{dt} = \sum_m \left(\frac{\partial r_k}{\partial n_{m,k}}\right)\frac{dn_{m,k}}{dt}, \qquad m = H_2O, H_2SO_4 \tag{47}$$

where

$$\frac{\partial r_k}{\partial n_{m,k}} = \frac{\overline{MW}_m}{4\pi\rho_{sol}r_k^2} \tag{48}$$

The condensation and evaporation processes control the weight fraction of H_2SO_4 in the liquid solution ($W_{H_2SO_4}$), on which many thermodynamic quantities depend, e.g., the saturation vapor pressure in equation (40). Therefore, it is necessary to determine the evolution of $W_{H_2SO_4}$. Starting from its definition

$$W_{H_2SO_4,k} = \frac{\overline{MW}_{H_2SO_4} \times n_{H_2SO_4,k}}{\sum_m \overline{MW}_m \times n_{m,k}}, \qquad m = H_2O, H_2SO_4 \tag{49}$$

where $n_{m,k}$ is the mole number of species m in the droplets of size bin k, and the mass of the liquid droplets in the same bin is $\sum_m \overline{MW}_m \times n_{m,k} = 4\pi\rho_{sol}r_k^3/3$. Differentiating equation (49) with respect to time and invoking equations (47) and (48) leads to

$$\frac{dW_{H_2SO_4,k}}{dt} = \frac{3}{r_k}\left[\left(\frac{dr_k}{dn_{H_2SO_4,k}}\right)\frac{dn_{H_2SO_4,k}}{dt} - W_{H_2SO_4,k}\frac{dr_k}{dt}\right] \tag{50}$$

Using a semi-implicit formula, the result is

$$W^t_{H_2SO_4,k} = \frac{W^{t-h}_{H_2SO_4,k} + h\frac{3}{r_k}\left[\frac{dr_k}{dn_{H_2SO_4,k}}\frac{dn_{H_2SO_4,k}}{dt}\right]}{1+h\frac{3}{r_k}\frac{dr_k}{dt}} \tag{51}$$

4.7. Effects of Microphysical processes on Species Evolution

The conservation equations of gas-phase H_2SO_4, SO_3 and H_2O will have additional source/sink terms due to the microphysical processes described above, i.e.,

$$\frac{dC_{H_2O}}{dt} = \dot{w}'''_{H_2O} - J_{hom} n^*_{tot}(1-x^*) - \sum_{i=1}^{M_B} \frac{dn_{H_2O,i}}{dt} N_{H_2SO_4-H_2O,i} - \sum_{i=1}^{M_B} \theta_i \frac{dn_{H_2O,i}}{dt} N_{soot,i} \quad (52)$$

$$\begin{aligned}\frac{dC_{H_2SO_4}}{dt} = \dot{w}'''_{H_2SO_4} - J_{hom} n^*_{tot} x^* - \sum_{i=1}^{M_B} \frac{dn_{H_2SO_4,i}}{dt} N_{H_2SO_4-H_2O,i} \\ - \sum_{i=1}^{M_B} \theta_i \frac{dn_{H_2SO_4,i}}{dt} N_{soot,i} \\ -.25\alpha\bar{c} C_{H_2SO_4} \sum_{i=1}^{M_B} \pi d^2_{soot,i} N_{soot,i} \\ \times(1-\theta_i)\end{aligned} \quad (53)$$

$$\frac{dC_{SO_3}}{dt} = \dot{w}'''_{SO_3} - .25\alpha\bar{c} C_{SO_3} \sum_{i=1}^{M_B} \pi d^2_{soot,i} N_{soot,i} \times(1-\theta_i) \quad (54)$$

It is noted here that, there also exists other models for taking into account the effects of particle microphysical processes on the gas species. For example, in reference [20], Yelvington used the following relationship [21] to represent the rate of adsorption of H_2SO_4 by soot per aerosol

$$B_{H_2SO_4}(r_k) = \frac{4\pi r_k^2 D_{H_2SO_4}}{4D_{H_2SO_4}/(\beta_{c,H_2SO_4} v_{H_2SO_4}) + r_k^2/(r_k+\lambda_k)} \frac{p_{H_2SO_4}}{R_u T} \quad (55)$$

It is a function of soot particle radius, temperature, and pressure. In addition, $D_{H_2SO_4}$, β_{c,H_2SO_4}, $v_{H_2SO_4}$, and $p_{H_2SO_4}$ are the diffusivity, molecular accommodation coefficient, gas mean speed, and partial pressure of species H_2SO_4; and λ_k and r_k are the mean free path and radius of soot particle in size bin k.

Similarly, the rate of condensation of a volatile species, α, per wetted aerosol is given by [21] as

$$C_\alpha(r_k)[mol/s] = \frac{4\pi r_k^2 D_\alpha}{4D_\alpha/(\beta_{c,\alpha} v_\alpha) + r_k^2/(r_k+\lambda_k)} \frac{p_\alpha - p^\infty_{\alpha,k}}{R_u T} \quad (56)$$

where α is any volatile species, and $p^\infty_{\alpha,k}$ the vapor pressure above a flat surface. Using the vapor pressure above a flat surface ignores the Kelvin effect, hence underestimates the timescale for condensation. Since the driving force for condensation is ($p_\alpha - p^\infty_{\alpha,k}$), condensation will not occur if the partial pressure is below the vapor pressure. Thus, it is very important that the correct saturation vapor pressure is used.

5. Applications

The numerical platform is a NASA in-house code for simulating turbulent combustion in propulsion systems. A detailed description of this code can be found in several reports [22,23,24]. Its enhancements for post-combustor trace chemistry modeling and simulation are reported by Wey and Liu [25]. Under the current effort, we have further implemented the microphysical models for aerosol dynamics discussed in the previous sections into this analysis tool. In the following, its application to the turbine environment as well as to the components of particle sampling system are discussed.

Several investigations (e.g., Lukachko et al. [3]) have shown the important role of gas phase chemistry along the post combustor flow path in the production of sulfate and nitrate aerosol precursors. In particular, it has been suggested that multi-dimensional analysis needs be applied to the high-pressure turbine section, while one-dimensional simulations suffice for the remaining sections of the internal gas path.

It has also been known that strong modification in the temperature and pressure environment experienced by the particles in the sampling system can lead to different interpretations of the measurements aimed at characterizing the particle emissions of the exhaust. Therefore, there is a need to conduct higher fidelity computations to compliment these measurement studies and to assess the effects of sampling methodology.

Finite rate kinetic mechanisms developed for conditions intermediate between combustion and atmospheric chemistry have been used in the present work. More specifically, a mechanism involving 25 species and 74 reaction steps [26] was used for investigating a film cooled turbine blade; later, an improved mechanism involving 29 species and 73 reaction steps [3] was used for other applications. All simulations require the specification of species concentrations along the inflow boundary of the computational domain, we have followed the approach outlined in [3] to provide the estimation of these species initial conditions.

5.1. Film Cooled Turbine Blade

Film cooling injection is widely applied in the thermal design of turbomachinery, as it contributes to meet the requirements for reliability and life cycles of modern gas turbines operating at high temperature conditions. The film cooling influence on post-combustor trace chemistry has been computationally investigated by Wey and Liu [27], and a few selected results are cited here. Figure 1 presents the geometry and the grid used in the simulation. The coolant mass flow is about five percent of the mainstream hot gas mass flow. Five sets of computed results are assembled together to show the differences due to various codes as well as the cooling air injection. Data reduction has been performed to yield one dimensional distribution along the axis of the flow path by averaging the CFD results. The temperature distributions along the axis of flow path are depicted in Figure 2. It indicates that the impact of film cooling on the temperature is significant. It also suggests that the evaluation of transport properties affects the temperature more for the case with cooling air than the case without cooling air. NO distributions are shown in Figure 3. The mass fraction for the case with cooling air injection decreases significantly as the flow passes through the turbine vane. Figure 4 illustrates the SO_3 distributions. Its mass fraction with cooling air injection increases more than that without cooling air injection as the flow passes through the turbine vane.

5.2. First Stage of a High Pressure Turbine

As part of the NASA/QinetiQ (formerly DERA) emissions testing effort, two-dimensional calculations of the evolution of trace species in the first stage of a DERA high pressure turbine (HPT1) using the CNEW code were carried out by Lukachko et al. [3]. A relatively detailed description of the stage configuration and the specification of the inflow condition can be found in [3]. Under the present effort, the NCC code was used to calculate the evolution of trace species in the same HPT1 operating at two nominal power settings – cruise and maximum power – with similar high fuel sulfur levels. The results of the high sulfur cruise case will be briefly described here; additional results can be found in [28]. Figure 5 outlines the setup of the simulations, in particular, the transfer of the solution near the exit of the nozzle guide van (NGV) to the inlet of the rotor. Due to the wake of the NGV and the rotation of the rotor, the inlet flow of the rotor is non-uniform and unsteady. Figure 6 to Figure 9 present the fields of the temperature, NO, NO_2, and SO_3, respectively. In addition to the contour plot which is a snapshot at some instant, the area-averaged values also are presented. These averaged values are steady in the NGV region but change with time in the rotor region. It is noted here that results of the CNEWT code were obtained by using the triangular meshes, and only the solutions at one time station are depicted in these figures. On the other hand, quadrilateral meshes were used in the code NCC, and solutions at several time stations are given. Depending on the variable, these temporal solutions may bunch together (e.g., T) or separate more clearly from each other (e.g., NO). In general, the solutions obtained by these two codes are quite comparable, except for the variable SO_3, the reason for this larger difference is not clear.

5.3. Particulate Matter Probe

Two particulate matter probes have been investigated: a low dilution probe and a high dilution probe. The diluent is N_2. For the low dilution probe, the tip portion of the inlet has an inner diameter of 0.0625 inch, followed by a short divergent section; the diameter at the end of the inlet is 0.1875 inch, the length of the inlet is 0.6553 inch. For the high dilution probe, its inlet is a straight tube with an inner diameter of 0.044 inch, and a length of 1.2875 inch. In the present work, the computational domain of the low dilution probe is set to be 9.558 inch long, and the computational domain of the high dilution probe is chosen to be 6.456 inch long. The flow field of the low dilution probe was analyzed with an inflow total pressure of 49699 Pa, and inflow total temperature of 835.78 K. The mass flux of the N_2 diluent is 48 $kg\ m^{-2}s^{-1}$ at a temperature of 423 K. The exit pressure of the probe is set to be 19545 Pa, the wall temperature is set to a fixed value of 423 K. The computed dilution factor by mass is about 6.9, which is at the high end of the operation of a low dilution probe. Figure 10 indicates that a stagnation zone appears in the downstream region of the merged inlet stream and the diluent, while another flow stagnation zone sits next to the divergent wall of the inlet tube. These flow features will adversely impact the sampling functionality of the probe. Subsequently, the same flow conditions were used to evaluate the high dilution probe. However, due to the difference in size from the low dilution probe, the computed dilution factor by mass now is 25.8. The velocity vector fields of these two probes are compared in Figure 11. The mixing between the sampled stream and the diluent in these two probes are compared in Figure 12. The mixing is illustrated by the mass fraction of the sampled

stream in the mixture. It is evident that the high dilution probe is much more suitable for the given sampling condition.

Since the high dilution probe has been extensively used in the Aircraft Particle Emissions eXperiment (APEX), additional simulations have been performed for the high dilution probe. Conditions for the simulations are listed below:

- The engine operates at 65% power setting, and the probe is located at 1 meter downstream of the engine exit.
- A post combustor trace chemistry kinetic mechanism having 29 species and 73 reaction steps is used.
- Soot entering the probe has a number density of 1.0×10^{11} particles per cubic meter, it has a log-normal distribution with a median diameter of 40 nm and a standard deviation of 1.5.
- At the entrance of the probe, the pressure of the sampled gas is 101350 Pa, the static temperature is 720 K, and the speed is 210 meters per second. Therefore, the total pressure is 112515 Pa, and the total temperature is 742 K.
- The static temperature of the diluent N_2 is 290 K, the diluent mass flux is 110 $kgm^{-2}s^{-1}$, and the targeted dilution factor by mass is 24.
- The static pressure of the mixture at the exit of the computational domain is 81000 Pa. The temperature of the probe wall is set to 320 K.
- Aerosol size distribution is divided into 12 bins ($M_B = 12$), the diameter of particles in the smallest bin is 3 nm. Soot particles, H_2SO_4-H_2O droplets, and the mixture of them are included in the calculations. Consequently, a total of 72 equations are solved for each mesh cell.

Since the particle size distribution at the entrance of the probe is assumed to be log-normal, the following formula is used to discretize the continuous function into stepwise function, for size bin k:

$$N_k = \frac{N_{total}}{\sqrt{2\pi}\ln\sigma_g}\exp\left[-\frac{(\ln d_{p,k} - \ln d_{p,g})^2}{2\ln^2\sigma_g}\right]\frac{\Delta d_{p,k}}{d_{p,k}} \tag{57}$$

where N_{total} is the total number of particles of all sizes per m^3 of the exhaust gas, σ_g is the geometric standard deviation, $d_{p,g}$ is the median diameter of particles in meter, $d_{p,k}$ is the diameter of the particles in size bin k.

The H_2SO_4-H_2O nucleation rate depends highly on temperature, relative humidity, and H_2SO_4 concentration. The following empirical criterion [29] is used to decide whether H_2SO_4-H_2O nucleation commences:

$$C_{crit} = 0.16\exp(0.1T - 3.5\mathrm{RH} - 27.7) \tag{58}$$

where T is in degree K, RH is the relative humidity on a scale from 0 to 1, and C_{crit} is in $\mu g\ m^{-3}$. When the gas-phase concentration of H_2SO_4 exceeds C_{crit}, the nucleation of H_2SO_4-H_2O droplets starts. Sample results from these simulations are presented in Figure 13. While the number density of soot with 66 nm diameter remains essentially

unchanged along the probe length, the results indicate the emergence of H_2SO_4-H_2O droplets due to nucleation.

5.4. Sampling Line

Three-dimensional calculations have been conducted to capture the potentially important secondary flow effects by dividing the long sampling line into multiple shorter segments. Starting from the exit plane of the high dilution probe, a segment of the sampling line is simulated at first; the results at the exit plane of this segment are then used as the inlet profiles for the next segment, and so on. Two configurations have been investigated. The first one consists of two segments of a simple straight tube. The second one consists of a straight tube segment followed by a Z-shaped tube segment. Figure 14 presents the temperature distribution along the center line of the probe as well as along the center line of the sampling line segments. The temperature inside the probe drops rapidly because of the dilution, while the temperature in the sampling line is very close to the imposed wall temperature which is kept at 310 K. In Figure 15, the mass fraction distribution of species H_2SO_4 is shown. Due to a sudden expansion in volume from the end of the probe to the beginning of the sampling line, a rapid change is observed (the typical internal diameter of a sampling line is about 0.34 inch, the internal diameter at the end of the currently used AEDC/NASA high dilution probe is 0.249 inch). In Figure 16, the evolution of the soot particles with 33 nm diameter is shown. The loss of soot particles in the straight segment is smaller than the loss in the Z-shaped segment. Similar behavior is observed in Figure 17 for soot particles with 66 nm diameter. Figure 18 suggests that the process of H_2SO_4-H_2O nucleation as indicated by the emergence of droplets with 1 nm diameter starts from the inside of the probe and continues into the sampling line until the mass fraction of the gaseous H_2SO_4 levels off (see Figure 15). The results in Figure 19 suggest that the coagulation of H_2SO_4-H_2O droplets as indicated by the emergence of 2 nm droplets begins in the sampling line.

5.5. Pressure Reduction Chamber

The pressure of the exhaust gas at the exit of the combustor is much higher than the pressure in the ambient environment. A device which reduces the pressure of the sampled exhaust gas is often employed to meet the operating range of the particulate matter analyzers. A schematic of a typical pressure reduction vessel is shown in Figure 20. It is a cylinder-like device that has an inlet tube on the top and an exit tube in the bottom. The internal (inside) diameter, ID, of the inlet tube is denoted by a. The portion of the inlet tube inside the pressure reducer may be expended up to five degrees to slow down the drop of the incoming pressure and the temperature. The gap between the exit of the inlet tube and the entrance of the sample extraction tube is denoted by d. The diameter of the cylinder is denoted by S. In the current study, the internal diameter of the inlet tube is a = 0.09 inch and the diameter at the exit of the inlet tube is .2646 inch due to a five-degree expansion. The gap distance, d, is 2 inch; and the ID of the sample extraction tube is 0.34 inch. The diameter of the reducer is S = 3 inch; the overall length of the domain which includes the inlet tube, the chamber and the sample extraction tube is 35 inch (0.889 m). In the current study, instead of conducting three-dimensional calculations, axisymmetric simulations have been carried out by replacing the bleeding hole with a bleeding slot having the same opening area. Two cases are presented here to

show the chemical conversion and particle evolution in the device. The total pressure of the incoming gas are 65 and 255 psi, respectively. The total temperature is set to be 485 K for both cases. The shortest flow residence time is 21 ms for the case of 65 psi and 6.2 ms for the case of 255 psi. The exit pressure is set at 19.7 psi. The pressure at the bleeding location is 14.7 psi. The size distribution of the soot particle is prescribed to be log-normal, with median radius of 40 nm, modal widths of 1.5 and total number density of 10^{13} particle/m^3. The chemical composition of the inlet gas and the chemical kinematic mechanism are the same as those used in the study of particulate matter probe. The wall temperature of the inlet tube entering the vessel chamber is set to 400 F (477 K). The rest of the wall is either at a temperature of 450 K or insulated. The temperature distributions along a line which is 0.018 inch away from the center axis are shown in Figure 21. For the 65 psi case, the temperature is above 450 K from the inlet to the exit, hence the occurrence of the nucleation of H_2SO_4-H_2O droplets is not possible. For the 255 psi case, the temperature has dropped to near 250 K at the end of the inlet tube. The distributions of H_2SO_4 mass fraction along the 0.018-inch line are shown in Figure 22. The increase of the mass fraction occurs in the straight portion of the inlet tube outside of the chamber region. It also indicates that the chamber has little influence on the evolution of H_2SO_4. In Figure 23, the number density distribution, in $\log_{10}$ scale, of the soot particles is shown for the 65 psi case. The influence of the chamber on the size distribution is very mild. Figure. 24 is for the 255 psi case, the influence of the chamber on the size distribution of the soot particles is more noticeable. Figure 25 shows that, due to the relatively large dropping of the temperature, the nucleation of H_2SO_4-H_2O droplets is significant in the case of 255 psi, in addition, the coagulation of smaller droplets to form the larger ones also occurs.

6. Summary

To better understand the formation and subsequent development of gaseous pollutants, particulate pollutants and their precursors of aviation-sourced emissions, it is necessary to adopt approaches which combine the use of accurate measurement and high-fidelity modeling and simulation. The development of such a CFD based multi-dimensional modeling and simulation tool which accounts for and integrates fluid dynamics, chemistry and particle microphysics relevant to the aircraft emissions is elucidated in the present paper. Its capabilities have been demonstrated by the results of several applications in environments representative of post-combustor flow path and sampling system. This represents a first step towards the long-term goal of establishing physically based tools that can be used to handle fundamental processes acting on length/time scales relevant to practical sampling and measurement. Obviously, the tool developed under the current effort must be further validated by data from systematic and careful parametric measurements. At the present time, measurements aimed at providing comprehensive data for the purpose of model development/improvement and validation are lacking. This is one area which needs to be strengthened by the research community. In addition to validating and further improving the existing predictive capabilities, our near term efforts will also include the modeling and simulation in the jet engine plume environment and the modeling of soot formation.

References

[1] Vancassel, X., Sorokin, A., Mirabel, P., Petzold, A., and Wilson, C., "Volatile Particles Formation During PartEmis: A Modelling Study," Atmos. Chem. Phys., 4, 439-447, 2004.
[2] Vouitsis, E., Ntziachristos, L., and Samaras, Z., "Modelling of Diesel Exhaust Aerosol During Laboratory Sampling," Atmospheric Environment, 39, 1335-1345, 2005.
[3] Lukachko, S. P., Waitz, I. A., Miake-Lye, R. C., and Brown, R. C., "Engine Design and Operational Impacts on Particulate Matter Precursor Emissions," GT2005-69112, ASME Turbo Expo 2005, June 6-9, Reno-Tahoe, Nevada.
[4] Dakhel, P. M., Lukachko, S. P., Waitz, I. A., Miake-Lye, R. C., and Brown, R.C., "Post-Combustion Evolution of Soot Properties in An Aircraft Engine," GT2005-69113, ASME Turbo Expo 2005, June 6-9, Reno-Tahoe, Nevada.
[5] Gelbard, F. and Seinfeld, J. H., "The General Dynamics Equation for Aerosols," J. Colloid Interface Sci. 68(2):363-382, 1979.
[6] Peterson, T. W., Gelbard F., and Seinfeld, J. H., "Dynamics of Source-Reinforced, Coagulating, and Condensing Aerosols," J. Colloid Interface Sci. 63:426-445, 1978.
[7] Doyle, G. J., "Self Nucleation in the Sulfuric Acid-Water system," J. Chem. Phys., 35, 795-799, 1961.
[8] Kärcher, B., "On the Potential Importance of Sulfur-Induced Activation of Soot Particles in Nascent Jet Aircraft Exhaust Plumes," Atmospheric Research 46(1998) 293-305.
[9] Wang, Z., "Numerical Modeling of Chemistry, Turbulent Mixing and Aerosol Dynamics in Near-Field Aircraft Plumes," Ph.D. dissertation, University of California at Berkeley, 1998.
[10] Brock, J. R., "On the Theory of Thermal Forces Acting on Aerosol Particles," J. Colloid Sci., 17, 768-780, 1962.
[11] Elperin, T., Kleeorin, N., and Rogachevskii, I., "Turbulent Thermal Diffusion of Small Inertial Particles," Physical Review Letters, Vol. 76, Number 2, January 1996.
[12] Waldmann L., and Schmitt, K. H., "Thermophoresis and Diffusiophoresis of Aerosols, Chapter VI," in C. N. Davies (Ed.) Aerosol Science, 1966, Academic, New York.
[13] Fuchs, N. A., "The Mechanics of Aerosols," Pergamon Press, Oxford, 1964.
[14] Jacobson, M., "Fundamentals of Atmospheric Modeling," Second Edition, Cambridge University Press, 2005.
[15] Jacobson, M. and Turco, R. P., "Modeling Coagulation among Particles of Different Composition and Size," Atmospheric Environment Vol. 28, No. 7, pp. 1327-1338, 1994.
[16] Kulmala, M., Laaksonen, A., and Pirjola, L., "Parameterizations for Sulfuric Acid/Water Nucleation Rates," J. Geophys. Res., 103, 8301-8308, 1998.
[17] Vehkamäki, H., Kulmala, M., Napari, I., Lehtinen, K. E. J., Timmreck, C., Noppel M., and Laaksonen, A., "An Improved Parameterization for Sulfuric Acid-Water Nucleation Rates for Tropospheric and Stratospheric Conditions," Journal of Geophysical Research, Vol. 107 NO. D22, 4622, 2002.
[18] Vehkamäki, H., Kulmala, M., Lehtinen, K. E. J., and Noppel, M., "Modelling Binary Homogeneous Nucleation of Water-Sulfuric Acid Vapours: Parameterizaion for High Temperature Emissions," Environ. Sci. Technol. 2003, 37, 3392-3398.

[19] Fukuta, N. and Walter, L. A., "Kinetics of Hydrometeor Growth from a Vapor-Spherical Model," J. Atmos. Sci., 27 1160-1172, 1970.
[20] Yelvington, P. E., "Analysis of Chemistry and Microphysics in Sampling Probes for Emissions Measurements from Jet Engines," unpublished report, Department of Chemical Engineering, MIT, Cambridge MA, 2004.
[21] Brown, R. C., Miake-Lye, R.C., Anderson, M.R., Kolb, C.E., and Resch, T.J., "Aerosol Dynamics in Near-Field Aircraft Plumes," Journal of Geophysical Research, 101(D17):p.22,939-22,953, 1996.
[22] Chen, K.-H., Norris, A.T., Quealy, A., and Liu, N.-S., "Benchmark Test Cases for the National Combustion Code," AIAA Paper 98-3855, 1998.
[23] Ajmani, K., and Chen, K.-H., "Unsteady Flow Computations for the NCC," AIAA Paper 2001-0972, 2001.
[24] Liu, N.-S., "On the Comprehensive Modeling and Simulation of Combustion Systems," AIAA Paper 2001-0805, January 2001.
[25] Wey, T. and Liu, N.-S., "Current Status of Post-Combustor Trace Chemistry Modeling and Simulation at NASA Glenn Research Center," NASA TM-2003-212184, March 2003.
[26] Lukachko, S.P., Waitz, I.A., Miake-Lye, R.C., Brown, R.C. and Anderson, M.R., "Production of Sulfate Aerosol Precursors in The Turbine and Exhaust Nozzle of An Aircraft Engine," Journal of Geophysical Research, Vol. 103, NO.D13, Pages 16.159-16.174, July 20, 1998.
[27] Wey, T. and Liu, N.-S., "Film Cooling Flow Effects on Post-Combustor Trace Chemistry," ISABE-2003-1090, XVI International Symposium on Air Breathing Engines, August-September 2003. Also NASA TM-2003-212018, January 2003.
[28] Liu, N.-S. and Wey, T., "GRC Turbine Trace Chemistry Modeling," NASA Glenn Research Center UEET Tech Forum, October 2003, Westlake, Ohio.
[29] Seinfeld, J. H. and Pandis, S. N., "Atmospheric Chemistry and Physics: From Air Pollution to Climate Change," John Wiley & Sons, Inc. 1998.
[30] Preining, O., Wagner, P. E., Pohl, F. G., and Szymanski, W., "Heterogeneous Nucleation and Droplet Growth," University of Vienna, Institute of Experimental Physics. Vienna, Austria, 1981.
[31] Kulmala, M. and Laaksonen, A.J., "Binary nucleation of water–sulfuric acid system: Comparison of classical theories with different H_2SO_4 saturation vapor pressures," J. Chem. Phys. 93, 696-701, 1990.
[32] National Research Council, International Critical Tables of Numerical Data Physics, Chemistry and Technology, vol. 1 pp.56-57, McGraw-Hill, New York, 1928.
[33] Zeleznik, F. J., "Thermodynamic Properties of the Aqueous Sulfuric Acid System to 350K," J. Phys. Chem. Ref. Data 20, 1157-1200, 1991.
[34] Pruppacher, H. R. and Klett, J. D., "Microphysics of Clouds and Precipitation," Kluwer Academic Publ., Dordrecht, Holland, 1997.
[35] Davis, E. J., "Transport Phenomena with Single Aerosol Particles", Aerosol Sci. Technol., 2. 121-144, 1983.

Appendix A — Parameterized Homogeneous Nucleation Rate

Because the classical theory is often unreliable for predicting the nucleation rates, nucleation parameterizations have been developed to replace the classical theory.

A.1. Parameterization of Low Temperature Nucleation

This parameterization is valid for temperature ranging from $190.15-305.15K$ and relative humidity (RH) ranging from $0.01-100\%$. The mole fraction of sulfuric acid in the critical cluster is given by

$$\begin{aligned} x^* = {} & .740997 - .00266379T - 0.00349998\ln(N_{sa}) + .0000504022T\ln(N_{sa}) \\ & + .00201048\ln\left(\frac{\mathrm{RH}}{100}\right) - .000183289T\ln\left(\frac{\mathrm{RH}}{100}\right) \\ & + .00157407\left[\ln\left(\frac{\mathrm{RH}}{100}\right)\right]^2 - .0000179059T\left[\ln\left(\frac{\mathrm{RH}}{100}\right)\right]^2 \\ & + .000184403\left[\ln\left(\frac{\mathrm{RH}}{100}\right)\right]^3 - 1.50345\times10^{-6}T\left[\ln\left(\frac{\mathrm{RH}}{100}\right)\right]^3 \end{aligned}$$

where ln is the nature log function, N_{sa} is the number density of gaseous sulfuric acid ($molec./cm^3$), T is the absolute temperature in K, and RH is the relative humidity in percent ($100\times p_{H_2O}/p_{H_2O}^{saturation}$).

The nucleation rate is given by an exponential of a third-order polynomial of $\ln(\frac{\mathrm{RH}}{100})$ and $\ln(N_{sa})$,

$$\begin{aligned} J_{hom}[particle\ cm^{-3}s^{-1}] = \exp\{ \ & a + b\cdot\ln\left(\frac{\mathrm{RH}}{100}\right) \\ & + c\cdot\left[\ln\left(\frac{\mathrm{RH}}{100}\right)\right]^2 + d\cdot\left[\ln\left(\frac{\mathrm{RH}}{100}\right)\right]^3 \\ & + e\cdot\ln(N_{sa}) + f\cdot\ln\left(\frac{\mathrm{RH}}{100}\right)\ln(N_{sa}) \\ & + g\cdot\left[\ln\left(\frac{\mathrm{RH}}{100}\right)\right]^2\ln(N_{sa}) + h\cdot\left[\ln(N_{sa})\right]^2 \\ & + i\cdot\ln\left(\frac{\mathrm{RH}}{100}\right)\left[\ln(N_{sa})\right]^2 + j\cdot\left[\ln(N_{sa})\right]^3 \ \} \end{aligned}$$

where the coefficients $a\ldots j$ are functions of temperature and critical cluster mole fraction x^*

$$a = .14309 + 2.21956\cdot T - .0273911\cdot T^2 + .0000722811\cdot T^3 + 5.91822/x^*$$
$$b = .117489 + .462532\cdot T - .0118059\cdot T^2 + .0000404196\cdot T^3 + 15.7963/x^*$$
$$c = -.215554 - .0810269\cdot T + .00143581\cdot T^2 - 4.77580\times10^{-6}\cdot T^3 - 2.91297/x^*$$
$$d = -3.5885600 + .04950800\cdot T - .0002138200\cdot T^2 + 3.10801\times10^{-7}\cdot T^3 - .0293333/x^*$$

$$e = 1.1459800 - .600796 \cdot T + .00864245 \cdot T^2 - .0000228947 \cdot T^3 - 8.44985/x^*$$
$$f = 2.1585500 + .0808121 \cdot T - .000407382 \cdot T^2 - 4.01957 \times 10^{-7} \cdot T^3 + .721326/x^*$$
$$g = 1.62410 - .01601060 \cdot T + .0000377124 \cdot T^2 + 3.21794 \times 10^{-8} \cdot T^3 - .0113255/x^*$$
$$h = 9.716820 - .1150480 \cdot T + .000157098 \cdot T^2 + 4.00914 \times 10^{-7} \cdot T^3 + .71186/x^*$$
$$i = -1.05611 + .00903378 \cdot T - .0000198417 \cdot T^2 + 2.46048 \times 10^{-8} \cdot T^3 - .0579087/x^*$$
$$j = -.148712 + .00283508 \cdot T - 9.24619d - 6 \cdot T^2 + 5.00427 \times 10^{-9} \cdot T^3 - .0127081/x^*$$

The total number of molecules in the critical cluster, N_{tot}^*, is given by

$$\begin{aligned} N_{tot}^* = \exp\{ \; & ca + cb \cdot \ln\left(\frac{\mathrm{RH}}{100}\right) \\ & + cc \cdot \left[\ln\left(\frac{\mathrm{RH}}{100}\right)\right]^2 + cd \cdot \left[\ln\left(\frac{\mathrm{RH}}{100}\right)\right]^3 \\ & + ce \cdot \ln(N_{sa}) + cf \cdot \ln\left(\frac{\mathrm{RH}}{100}\right)\ln(N_{sa}) \\ & + cg \cdot \left[\ln\left(\frac{\mathrm{RH}}{100}\right)\right]^2 \ln(N_{sa}) + ch \cdot \left[\ln(N_{sa})\right]^2 \\ & + ci \cdot \ln\left(\frac{\mathrm{RH}}{100}\right)\left[\ln(N_{sa})\right]^2 + cj \cdot \left[\ln(N_{sa})\right]^3 \; \} \end{aligned}$$

where the coefficients *ca…cj* are functions of temperature and critical cluster mole fraction x^*

$$ca = -.00295413 - .097683400 \cdot T + .0010248500 \cdot T^2 - 2.18646 \times 10^{-6} \cdot T^3 - .101717000/x^*$$
$$cb = -.00205064 - .007585040 \cdot T + .0001926540 \cdot T^2 - 6.70430 \times 10^{-7} \cdot T^3 - .255774000/x^*$$
$$cc = 3.22308d - 3 + .000852637 \cdot T - 1.54757d - 5 \cdot T^2 + 5.66661 \times 10^{-8} \cdot T^3 + .03384440/x^*$$
$$cd = .047432300 - .000625104 \cdot T + 2.65066d - 6 \cdot T^2 - 3.67471 \times 10^{-9} \cdot T^3 - .000267251/x^*$$
$$ce = -.0125211000 + .005806550 \cdot T - .0001016740 \cdot T^2 + 2.88195 \times 10^{-7} \cdot T^3 + .094224300/x^*$$
$$cf = -.0385460000 - .000672316 \cdot T + 2.60288d - 6 \cdot T^2 + 1.19416 \times 10^{-8} \cdot T^3 - .008515150/x^*$$
$$cg = -.018374900 + .0001720720 \cdot T - 3.71766d - 7 \cdot T^2 - 5.14875 \times 10^{-10} \cdot T^3 + .000268660/x^*$$
$$ch = -.061997400 + 9.06958d - 4 \cdot T - 9.11728d - 7 \cdot T^2 - 5.36796 \times 10^{-9} \cdot T^3 - .007742340/x^*$$
$$ci = .012182700 - .0001066500 \cdot T + 2.53460d - 7 \cdot T^2 - 3.63519 \times 10^{-10} \cdot T^3 + .000610065/x^*$$
$$cj = .000320184 - .0000174762 \cdot T + 6.06504d - 8 \cdot T^2 - 1.42177 \times 10^{-11} \cdot T^3 + .000135751/x^*$$

The radius of the cluster in nanometers is given as a function of the mole fraction and the total number of molecules in the cluster:

$$r^*[nm] = \exp\left[-1.6524245 + 0.42316402x^* + .33466483\ln(N_{tot}^*)\right]$$

A.2. Parameterization of High Temperature Nucleation

This parameterization is valid for temperature ranging from $300.15 - 400.15K$ and relative humidity ranging from $1 - 100\%$. The mole fraction of sulfuric acid (or the acidity) in the critical cluster is given by

$$x^* = .847012 - 0.0029656T - 0.00662266\ln(N_{sa}) + .0000587835T\ln(N_{sa})$$
$$+.0592653\ln\left(\frac{\mathrm{RH}}{100}\right) - .000363192T\ln\left(\frac{\mathrm{RH}}{100}\right)$$
$$+.0230074\left[\ln\left(\frac{\mathrm{RH}}{100}\right)\right]^2 - .0000851374T\left[\ln\left(\frac{\mathrm{RH}}{100}\right)\right]^2$$
$$+.00217417\left[\ln\left(\frac{\mathrm{RH}}{100}\right)\right]^3 - 7.923\times10^{-6}T\left[\ln\left(\frac{\mathrm{RH}}{100}\right)\right]^3$$

where N_{sa} is the number density of gaseous sulfuric acid ($molec./cm^3$), T is the absolute temperature in K, and RH is the relative humidity in percent ($100\times p_{H_2O}/p_{H_2O}^{saturation}$).

The nucleation rate is given by an exponential of a third-order polynomial of $\ln(\frac{\mathrm{RH}}{100})$ and $\ln(N_{sa})$

$$J_{hom}[particle\ cm^{-3}s^{-1}] = \exp\{\ a + b\cdot\ln\left(\frac{\mathrm{RH}}{100}\right)$$
$$+c\cdot\left[\ln\left(\frac{\mathrm{RH}}{100}\right)\right]^2 + d\cdot\left[\ln\left(\frac{\mathrm{RH}}{100}\right)\right]^3$$
$$+e\cdot\ln(N_{sa}) + f\cdot\ln\left(\frac{\mathrm{RH}}{100}\right)\ln(N_{sa})$$
$$+g\cdot\left[\ln\left(\frac{\mathrm{RH}}{100}\right)\right]^2\ln(N_{sa}) + h\cdot\left[\ln(N_{sa})\right]^2$$
$$+i\cdot\ln\left(\frac{\mathrm{RH}}{100}\right)\left[\ln(N_{sa})\right]^2 + j\cdot\left[\ln(N_{sa})\right]^3\ \}$$

where the coefficients $a\ldots i$ are functions of temperature and critical cluster mole fraction x^*

$$a = -.00156975 - .134245\cdot T + .100507\cdot T^2 - .000460103\cdot T^3 + .187416/x^{*2} + .0104122/x^*$$
$$b = .00195077 + .168038\cdot T - .0225755\cdot T^2 + .0000827149\cdot T^3 + .0025029/x^{*2} + .0155215/x^*$$
$$c = .00015408 - .0280301\cdot T + .00154587\cdot T^2 - 4.52701\times10^{-6}\cdot T^3 + .0915323/x^{*2} + .0711652/x^*$$
$$d = -.00509267 - .00796846\cdot T + .0000446828\cdot T^2 - 8.79425\times10^{-8}\cdot T^3 + .133991/x^{*2} + .831112/x^*$$
$$e = -.0227223 - 1.56512\cdot T + .00380717\cdot T^2 + 1.64109d - 5\cdot T^3 + 1.29499/x^{*2} + .0474821/x^*$$
$$f = .00310646 + .304518\cdot T - .000564012\cdot T^2 - 2.03267\times10^{-6}\cdot T^3 - .351584/x^{*2} + .103749/x^*$$
$$g = .077543 - .00196315\cdot T - .0000130412\cdot T^2 + 6.62369\times10^{-8}\cdot T^3 + .011347/x^{*2} + .0972804/x^*$$
$$h = -.153143 + .0575392\cdot T - .000306511\cdot T^2 - 2.96097\times10^{-8}\cdot T^3 - .0982514/x^{*2} + .336286/x^*$$
$$i = -.552173 - .00207043\cdot T + .0000144032\cdot T^2 + 8.83\times10^{-9}\cdot T^3 + .0119833/x^{*2} - .0700025/x^*$$
$$j = .126544 - .00136029\cdot T + 5.90598d - 6\cdot T^2 - 4.1715\times10^{-9}\cdot T^3 + .00170807/x^{*2} - .0064323/x^*$$

The total number of molecules in the critical cluster, N_{tot}^*, is given by

$$N_{tot}^{*} = \exp\{\ ca + cb \cdot \ln\left(\frac{\mathrm{RH}}{100}\right) + cc \cdot \left[\ln\left(\frac{\mathrm{RH}}{100}\right)\right]^2 + cd \cdot \left[\ln\left(\frac{\mathrm{RH}}{100}\right)\right]^3 + ce \cdot \ln(N_{sa}) + cf \cdot \ln\left(\frac{\mathrm{RH}}{100}\right)\ln(N_{sa}) + cg \cdot \left[\ln\left(\frac{\mathrm{RH}}{100}\right)\right]^2 \ln(N_{sa}) + ch \cdot \left[\ln(N_{sa})\right]^2 + ci \cdot \ln\left(\frac{\mathrm{RH}}{100}\right)\left[\ln(N_{sa})\right]^2 + cj \cdot \left[\ln(N_{sa})\right]^3\ \}$$

where the coefficients *ca*…*cj* are functions of temperature and critical cluster mole fraction x^*

$$ca = 7.51024d - 6 + .000502054 \cdot T - .0000368602 \cdot T^2 + 1.08256 \times 10^{-6} \cdot T^3 - .000270282/x^*$$

$$cb = -4.30048d - 6 - .000730133 \cdot T + .0002520620 \cdot T^2 - 1.01648 \times 10^{-6} \cdot T^3 - .001142830/x^*$$

$$cc = -4.42156d - 6 - .002348600 \cdot T + 3.0065 \times 10^{-7} \cdot T^2 + 2.44797 \times 10^{-8} \cdot T^3 - .002502260/x^*$$

$$cd = -.000167057 + .000207504 \cdot T - 1.13013 \times 10^{-6} \cdot T^2 + 1.80268 \times 10^{-9} \cdot T^3 - .016824500/x^*$$

$$ce = .0000985954 + .004512850 \cdot T - .0000512557 \cdot T^2 + 4.60749 \times 10^{-8} \cdot T^3 - .002143180/x^*$$

$$cf = .0000636528 - .002885290 \cdot T + 6.51706 \times 10^{-6} \cdot T^2 + 2.32601 \times 10^{-8} \cdot T^3 - .001103190/x^*$$

$$cg = .000449239 + .0000689416 \cdot T - 3.50302 \times 10^{-7} \cdot T^2 + 1.07451 \times 10^{-10} \cdot T^3 + .001696460/x^*$$

$$ch = .000831844 - 5.35108 \times 10^{-6} \cdot T + 1.66432 \times 10^{-6} \cdot T^2 - 3.05108 \times 10^{-9} \cdot T^3 - .000306251/x^*$$

$$ci = .003553744 + .0000306009 \cdot T - 2.11004 \times 10^{-7} \cdot T^2 - 2.11436 \times 10^{-11} \cdot T^3 + .000749890/x^*$$

$$cj = -.001435340 + 7.85600 \times 10^{-6} \cdot T - 3.45128 \times 10^{-8} \cdot T^2 + 5.21547 \times 10^{-11} \cdot T^3 - .000021423/x^*$$

The radius of the cluster in nanometers is given as a function of the mole fraction and the total number of molecules in the cluster:

$$r^*[nm] = \exp\left[-1.6525507 + 0.45852848x^* + .33483673\ln(N_{tot}^*)\right]$$

Appendix B — Thermodynamic Properties

In order to solve the aerosol dynamics, various thermodynamic properties are needed for the calculation of the microphysical processes.

B.1. Saturation Pure Water Vapor Pressure

According to Preining et at. [30], the saturation vapor pressure ($N/m^2, T \ in \ K$) for pure water is

$$p_{0,H_2O}^{flat} = \exp\left\{77.34491296 - \frac{7235.424651}{T} - 8.2\ln T + 0.0057113T\right\}$$

B.2. Saturation Pure Sulfuric Acid Vapor Pressure

According to Kulmala and Laaksonen [31], the saturation vapor pressure ($N/m^2, T \ in \ K$) for pure sulfuric acid above a flat surface of H_2SO_4 liquid is

$$p_{0,H_2SO_4}^{flat} = 101325.0 \times \exp\{ \ -11.695 + 10156 \times [\ -\frac{1.}{T} + \frac{1.}{360.15} + \frac{0.38}{545} \times \left(1. + \ln(\frac{360.15}{T}) - \frac{360.15}{T}\right) \ ] \ \}$$

The range of the temperature is from190.15 K to 400.15 K.

B.3. Surface Tension of Sulfuric Acid and Water

The following fit gives the surface tension $\sigma(J/m^2)$ for all sulfuric acid solution as a function of the temperature T and the mole fraction x :

$$\sigma(x,T)[Jm^{-2}] = (a + bT_1) \cdot T_1^{1.256}$$

where

$$a(x) = .2358 - .529 \cdot x + 4.073 \cdot x^2 - 12.6707 \cdot x^3 + 15.3552 \cdot x^4 - 6.3138 \cdot x^5$$

$$b(x) = -.14738 + 0.6253 \cdot x - 5.4808 \cdot x^2 + 17.2366 \cdot x^3 - 21.0487 \cdot x^4 + 8.719 \cdot x^5$$

$$T_1(x,T) = 1 - \frac{T}{T_c}$$

The pseudo critical temperature $T_c(x)$ is given by

$$T_c(x) = 647.15 \cdot (1.0 - x)^2 + 900.0 \cdot x^2 + 3156.1860 \cdot x \cdot (1.0 - x)$$

Note that the extrapolation to higher or lower temperatures behaves smoothly.

B.4. Density of Sulfuric Acid Solution

For temperature ranging from 273 K to 373 K, the density $\rho_{sol}(kg/m^3)$ of the sulfuric acid solution is fitted to a polynomial function of temperature and sulfuric acid mass fraction x_m [32]:

$$\rho_{sol}(x_m,T) = (a(x_m) + b(x_m) \cdot T + c(x_m) \cdot T^2) \cdot 1000.0$$

Here T is the temperature of the liquid (K) and x_m is the mass fraction of sulfuric acid.

The coefficients $a(x_m)$, $b(x_m)$ and $c(x_m)$ are obtained from the following equations:

$$a(x_m) = .7681724 + 2.1847140 \cdot x_m + 7.163002 \cdot x_m^2 - 44.31447 \cdot x_m^3 + 88.75606 \cdot x_m^4 - 75.73729 \cdot x_m^5 + 23.43228 \cdot x_m^6$$

$$b(x_m) = 1.808225 \cdot 10^{-3} - 9.294656 \cdot 10^{-3} \cdot x_m - .03742148 \cdot x_m^2 + 0.2565321 \cdot x_m^3 - .5362872 \cdot x_m^4 + .4857736 \cdot x_m^5 - .1629592 \cdot x_m^6$$

$$c(x_m) = -3.478524 \cdot 10^{-6} + 1.335867 \cdot 10^{-5} \cdot x_m + 5.195706 \cdot 10^{-5} \cdot x_m^2 - 3.717636 \cdot 10^{-4} \cdot x_m^3 + 7.990811 \cdot 10^{-4} \cdot x_m^4 - 7.458060 \cdot 10^{-4} \cdot x_m^5 + 2.58139 \cdot 10^{-4} \cdot x_m^6$$

B.5. Partial Molar Volume in a Two-Component Solution

The Kelvin equation involves $\overline{v}_m$ (m^3/mol), i.e., the partial molar volume of species m in a two-component solution. Given the volume $\overline{v}$ and the mole fraction of component 2, i.e., x_2, the partial molar volumes $\overline{v}_1$ and $\overline{v}_2$ are computed from the volume change when mixing the pure components:

$$\overline{v}_1 = \overline{v} - \frac{\triangle \overline{v}}{\triangle x_2} \cdot x_2$$

and

$$\overline{v}_2 = \overline{v} - \frac{\triangle \overline{v}}{\triangle x_2} \cdot (x_2 - 1)$$

such that $(1 - x_2)\overline{v}_1 + x_2 \overline{v}_2 = \overline{v}$. The molar volume of a two-component solution is given by

$$\overline{v} = \frac{\overline{MW}_{sol}}{\rho_{sol}} = \frac{(1 - x_2)\overline{MW}_1 + x_2 \overline{MW}_2}{\rho_{sol}} \tag{B1}$$

The slope, $\frac{\triangle \overline{v}}{\triangle x_2}$, is computed by using the finite difference:

$$\frac{\triangle \overline{v}}{\triangle x_2} = \frac{\overline{v}'' - \overline{v}'}{x''_2 - x'_2}$$

where $\overline{v}''$ and $\overline{v}'$ are evaluated by slightly perturbing x_2 in Equation (B1).

B.6. Saturated Partial Pressure of H_2SO_4 and H_2O Vapors

The Kelvin equation also involves $P_{m,sat}^{flat}$, i.e., the saturated vapor pressure of species m over a flat liquid surface having the same composition as the droplet. It is defined as

$$p_{m,sat}^{flat} = \gamma_m x_m p_{0,m}, \qquad m = H_2O, H_2SO_4$$

where γ_m is the activity coefficient, $p_{0,m}$ is the saturation vapor pressure of pure

component m. The activity coefficients, γ_{H_2O} and $\gamma_{H_2SO_4}$, in a binary system can be expressed as

$$T \cdot \log \gamma_{H_2O} = \frac{A_{H_2O} x_{H_2SO_4}^2}{[x_{H_2SO_4} + B_{H_2O} x_{H_2O}]^2}$$

$$T \cdot \log \gamma_{H_2SO_4} = \frac{A_{H_2SO_4} x_{H_2O}^2}{[x_{H_2O} + B_{H_2SO_4} x_{H_2SO_4}]^2}$$

where T is the temperature in degree K, x is the mole fraction, and the coefficients A and B are given by Zeleznik [33]:

$$A_{H_2O} = 2.989 \times 10^3 - \frac{2.147 \times 10^6}{T} + \frac{2.33 \times 10^8}{T^2}$$

$$A_{H_2SO_4} = 5.672 \times 10^3 - \frac{4.074 \times 10^6}{T} + \frac{4.421 \times 10^8}{T^2}$$

$$B_{H_2O} = \frac{1}{B_{H_2SO_4}} = 0.527$$

B.7. Diffusivity of H_2SO_4 and H_2O Molecules

According to Pruppacher and Klett [34], the diffusivity of H_2O molecules (m^2/s) at temperature between 233 K and 313 K is given by

$$D_{v,H_2O} = 10^{-4} \times 0.211 \left(\frac{T}{T^0}\right)^1 .94 \left(\frac{P^0}{P}\right)$$

where T^0 = 273.15K, P^0 = 1013.25 mbar. Since $D_v \propto v\lambda_g$ and the mean thermal velocity $v \propto 1/\sqrt{\overline{MW}_v}$, $D_v \propto 1/\sqrt{\overline{MW}_v}$. Therefore, D_{v,H_2SO_4} can be obtained through

$$D_{v,H_2SO_4} = D_{v,H_2O} \times \frac{\sqrt{\overline{MW}_{H_2O}}}{\sqrt{\overline{MW}_{H_2SO_4}}}$$

Alternatively [35], D_{v,H_2SO_4} can be computed from

$$D_{v,H_2SO_4} = \frac{3}{8Ad^2\rho_g} \times \left[\frac{R_u T \overline{MW}_g}{2\pi}\left(\frac{\overline{MW}_{H_2SO_4} + \overline{MW}_g}{\overline{MW}_{H_2SO_4}}\right)\right]^{\frac{1}{2}}$$

where d is the diameter of a sulfuric acid molecule, commonly taken as $4.5 \times 10^{-}10m$, $\overline{MW}_{H_2SO_4}$ is its molecular weight ($kg/mole$), $\overline{MW}_g$ is the mass of carrier gas per mole ($kg/mole$), ρ_g is the density of carrier gas (kg/m^3) and A is the Avogadro's number ($= 6.02252 \times 10^{23} mole^{-1}$).

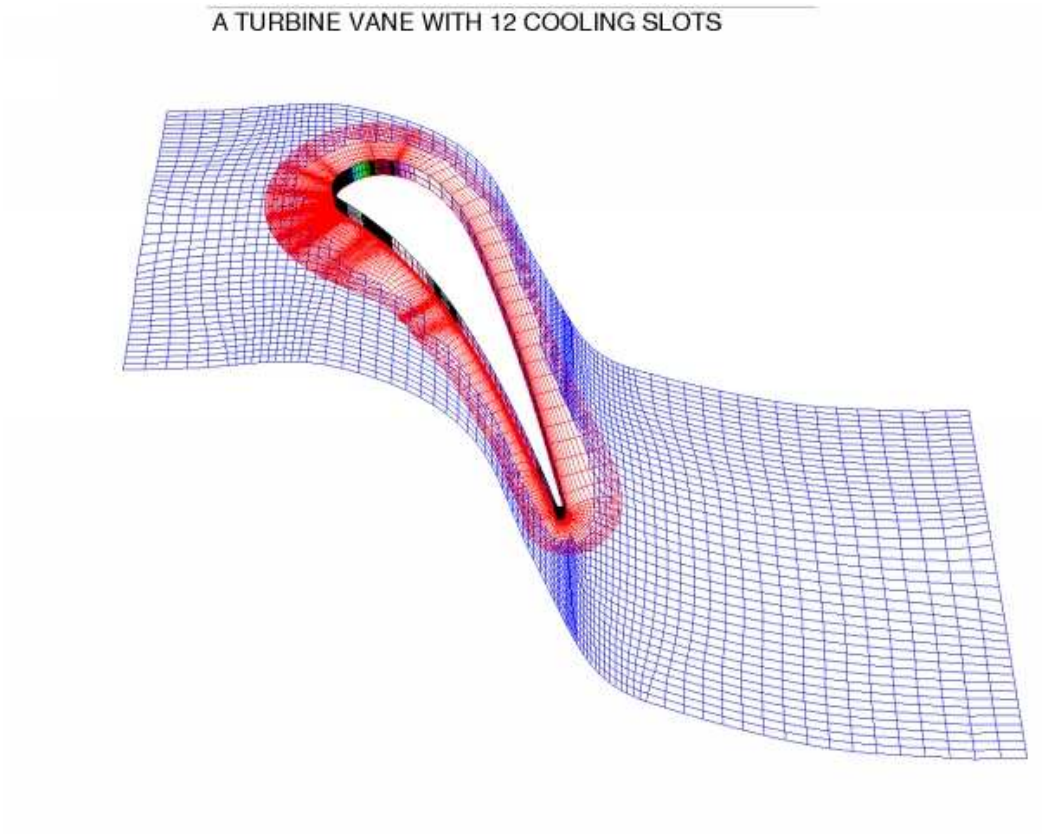

Figure 1: A two-block overset grid around the vane. (Thickness of vane is about .01m.)

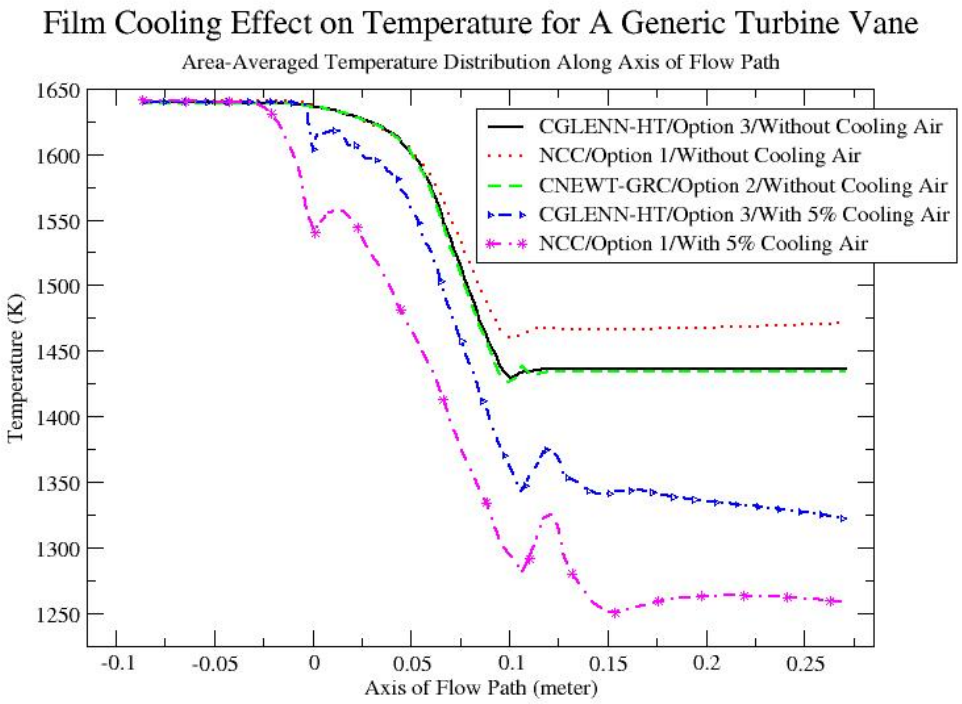

Figure 2: Comparison of area-averaged temperature distributions along the axis of flow path.

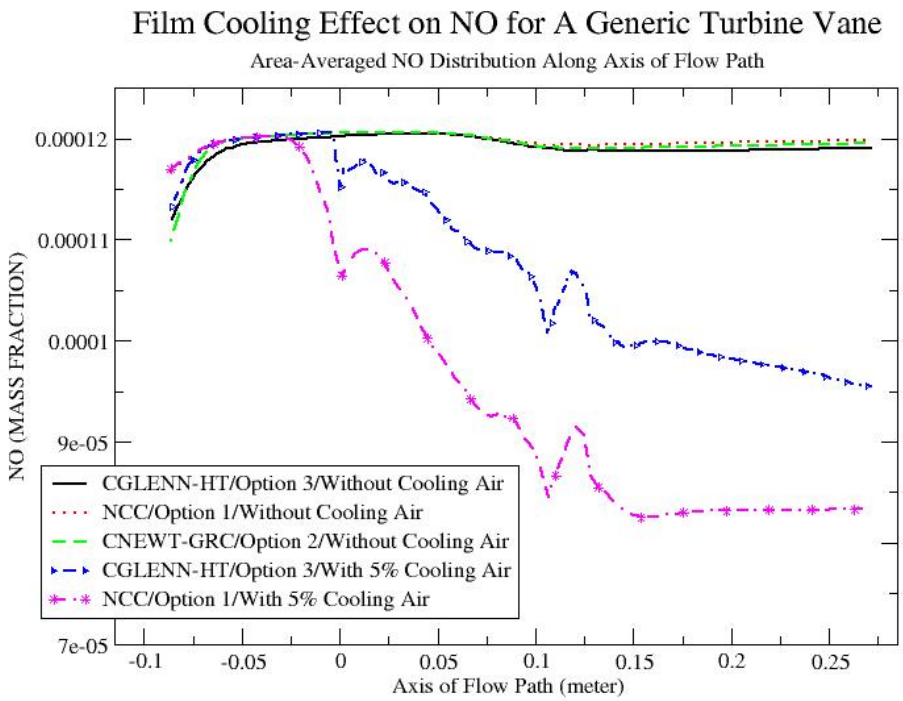

Figure 3: Comparison of area-averaged NO distributions along the axis of flow path.

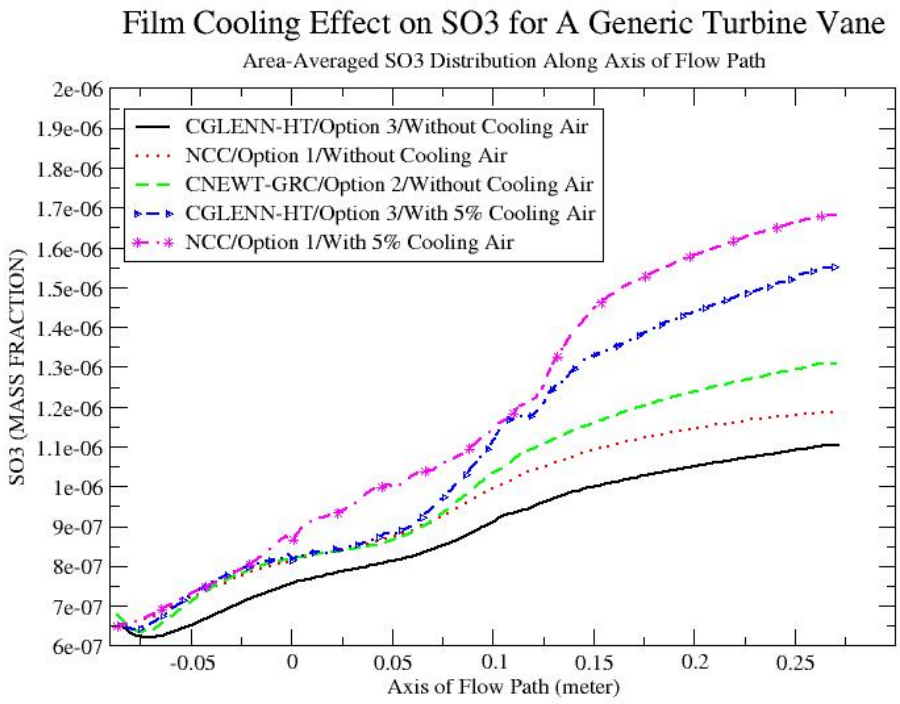

Figure 4: Comparison of area-averaged SO_3 distributions along the axis of flow path.

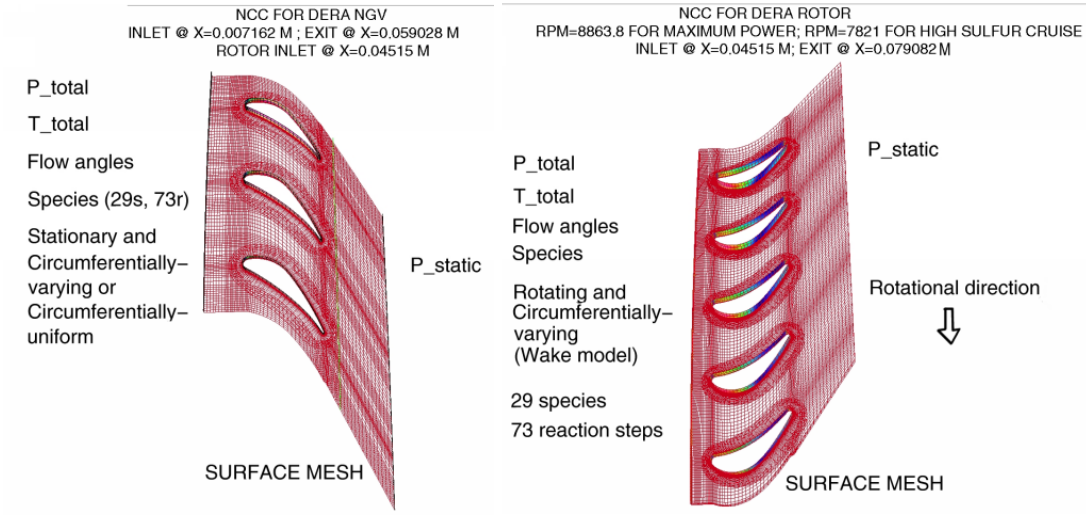

Figure 5 Boundary condition specification for 2-D unsteady HPT1 simulations

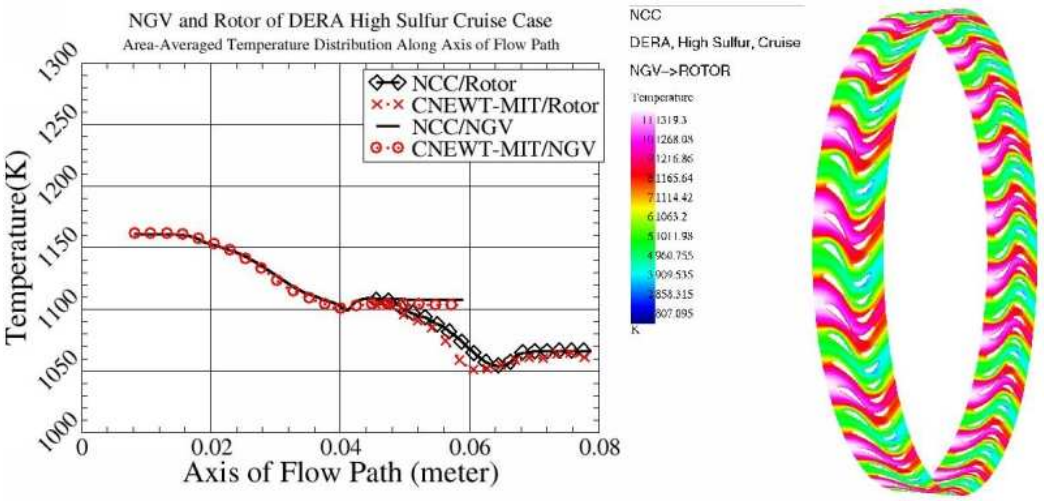

Figure 6 Area-averaged temperature distribution along the axis of flow path

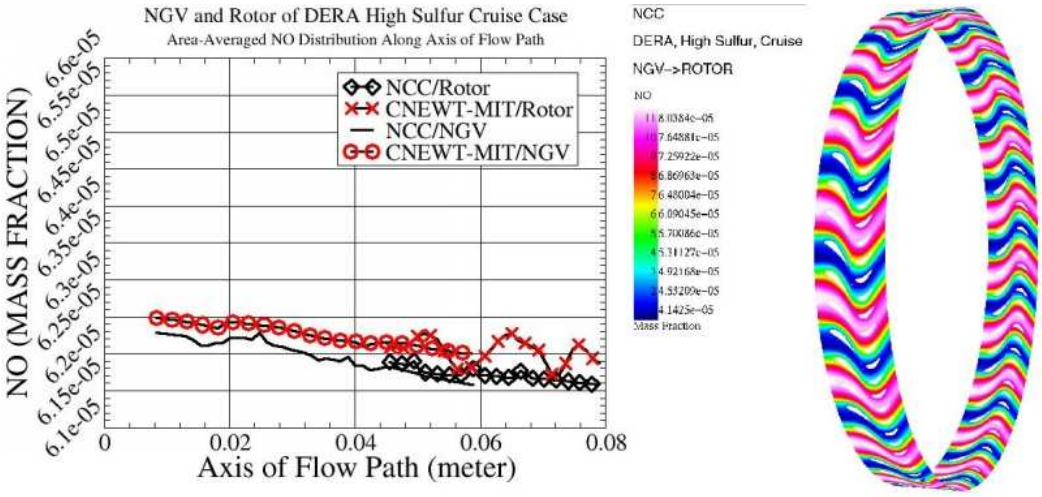

Figure 7 Area-averaged NO distribution along the axis of flow path

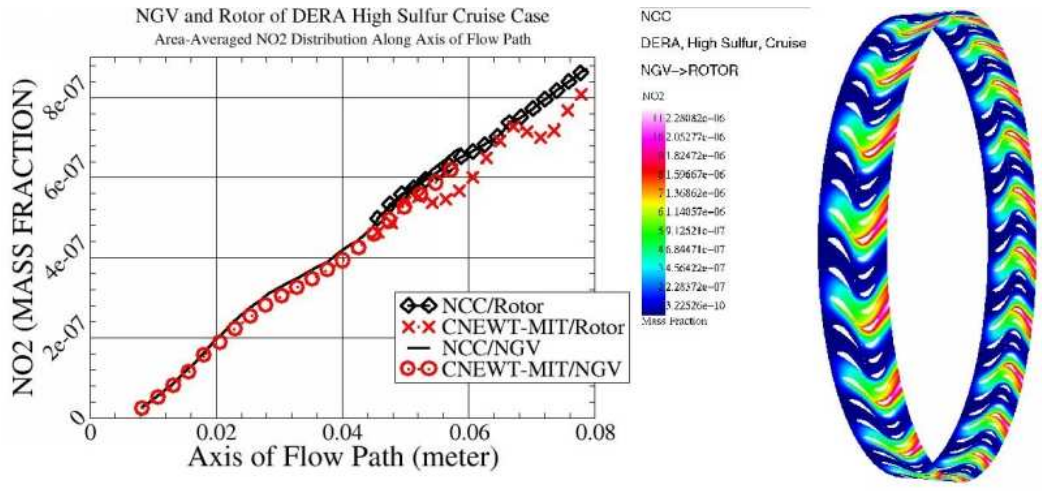

Figure 8 Area-averaged NO2 distribution along the axis of flow path

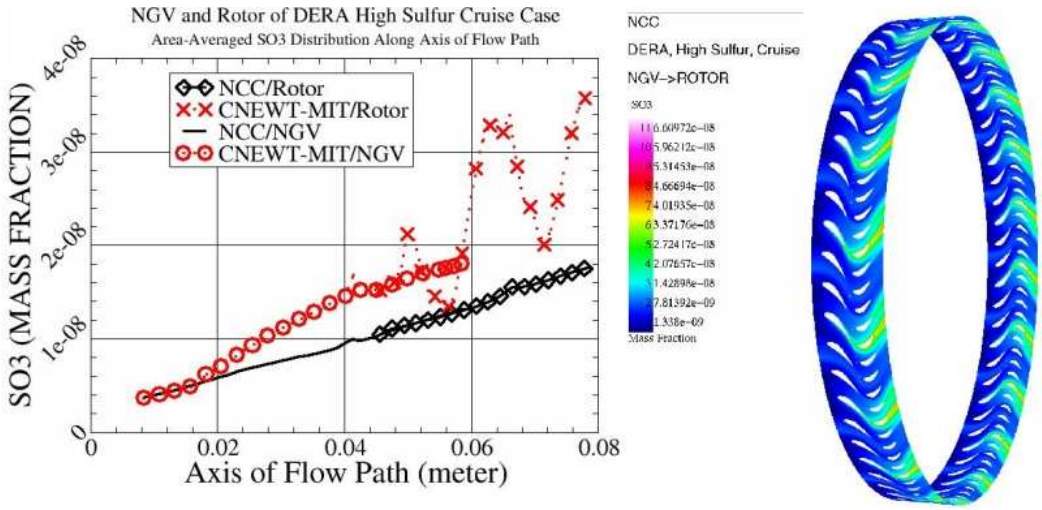

Figure 9 Area-averaged SO3 distribution along the axis of flow path

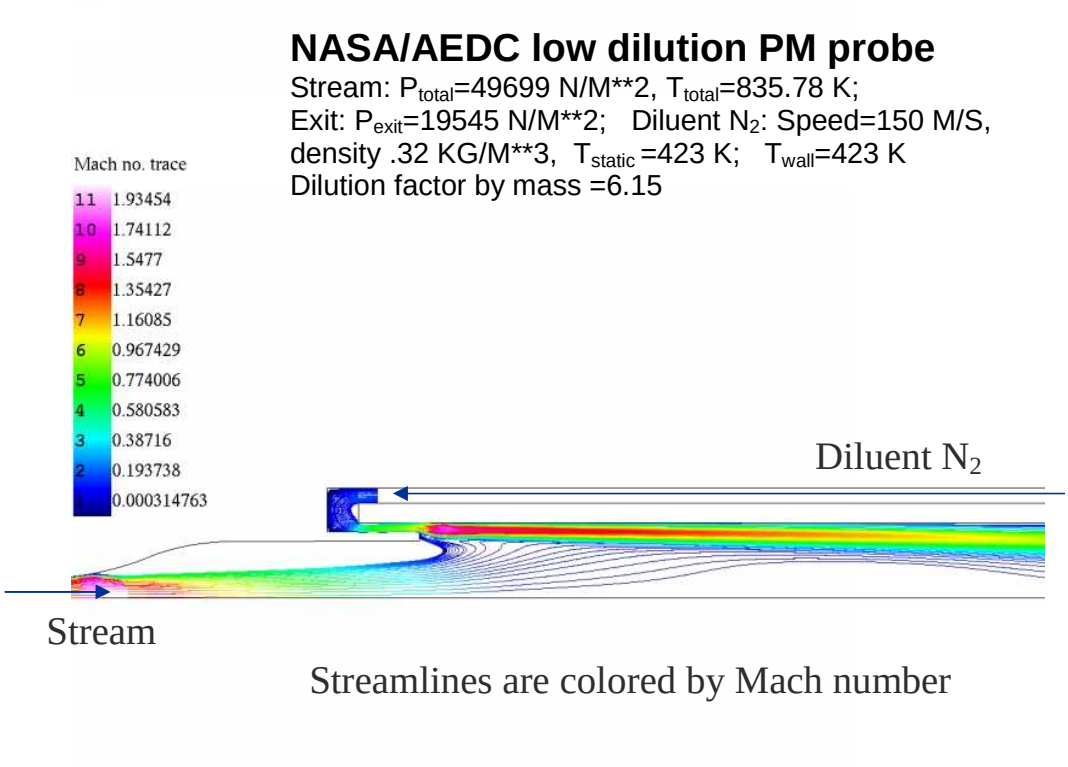

Figure 10 Streamlines of the low dilution PM probe

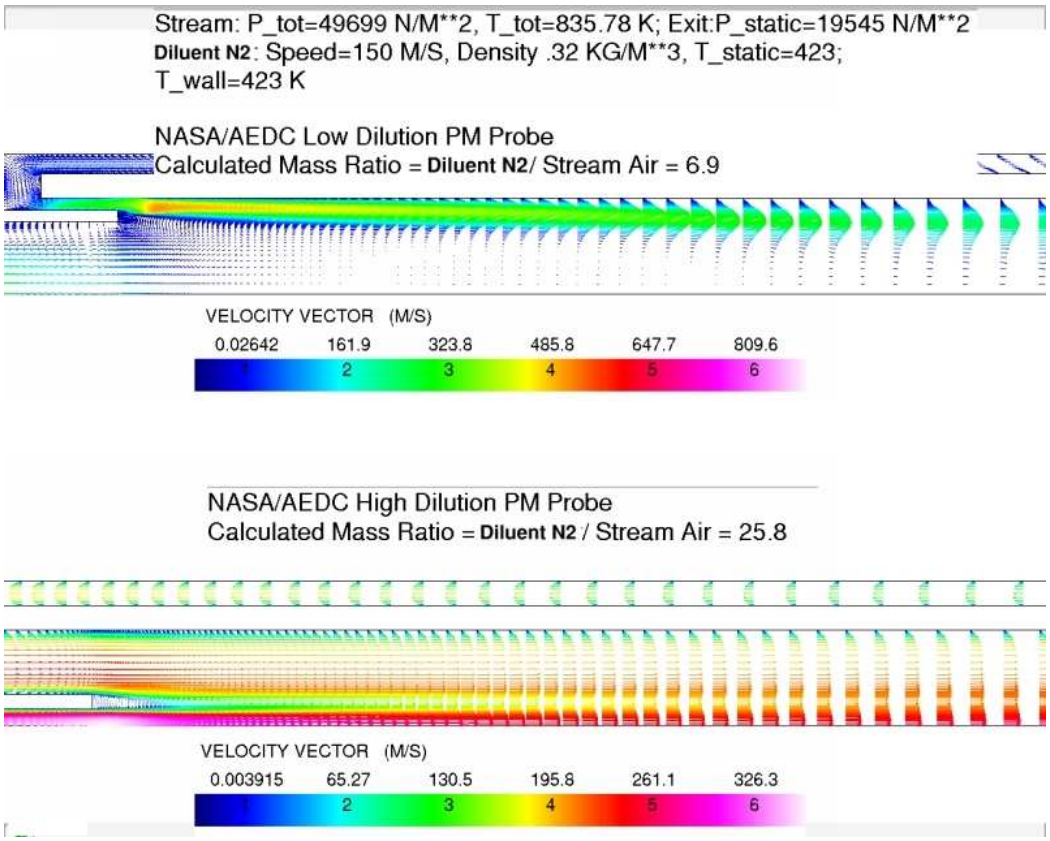

Figure 11 Velocity vectors of two different PM probes

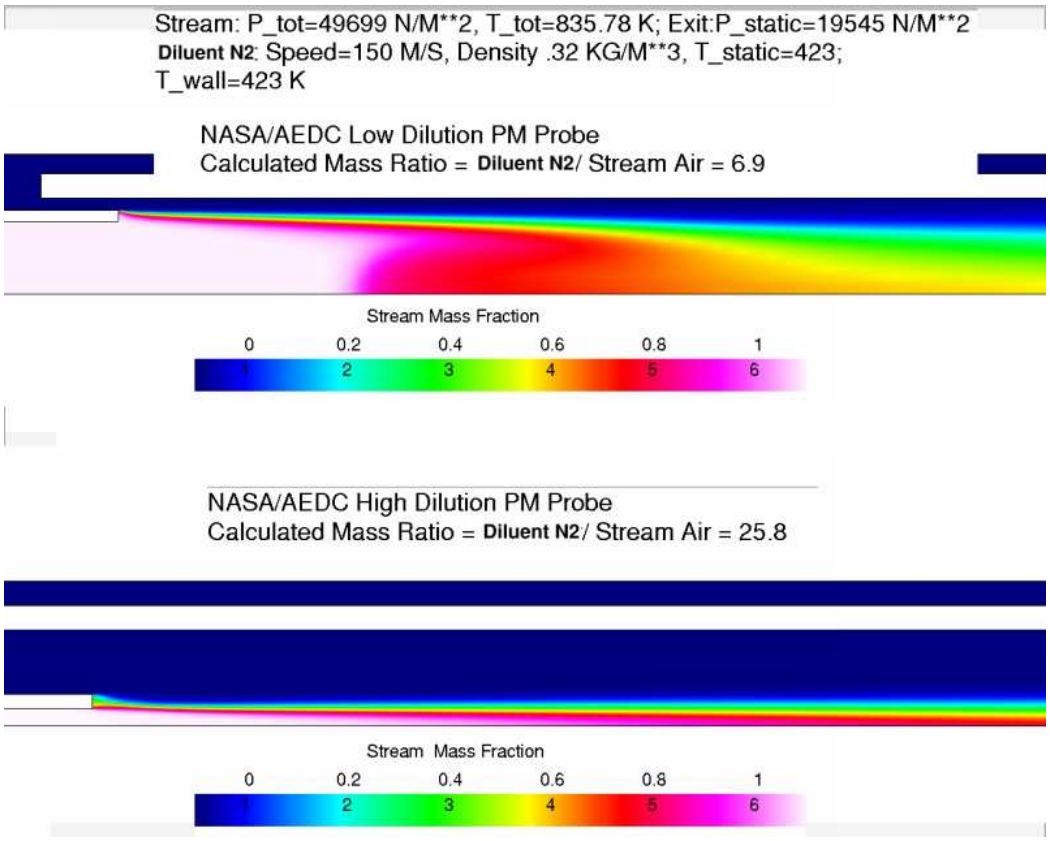

Figure 12 Mixing between the sampled stream and the diluent.

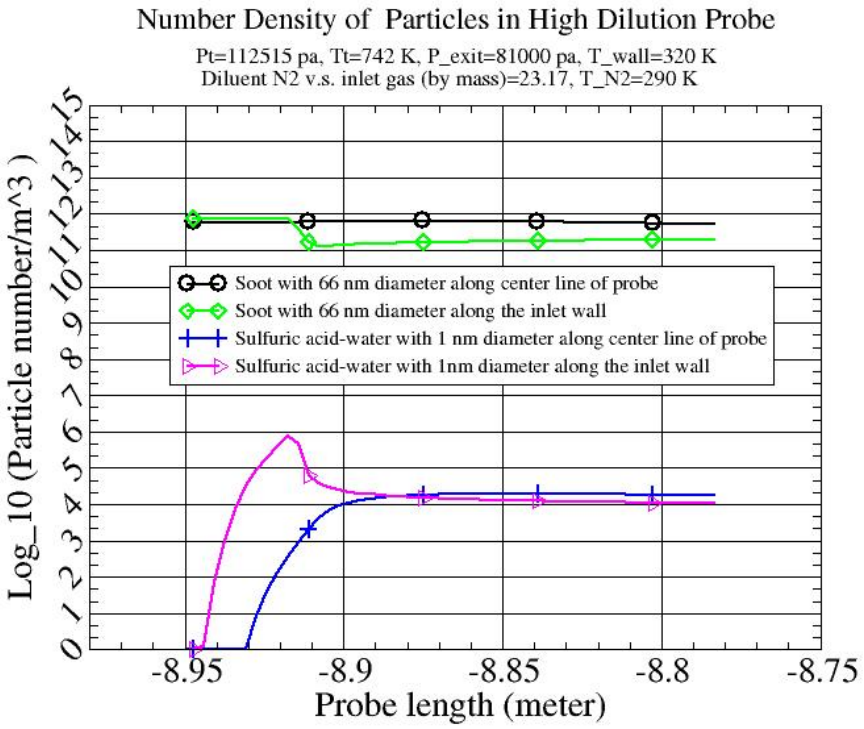

Figure 13 Soot evolution and H2SO4-H2O nucleation in high dilution probe.

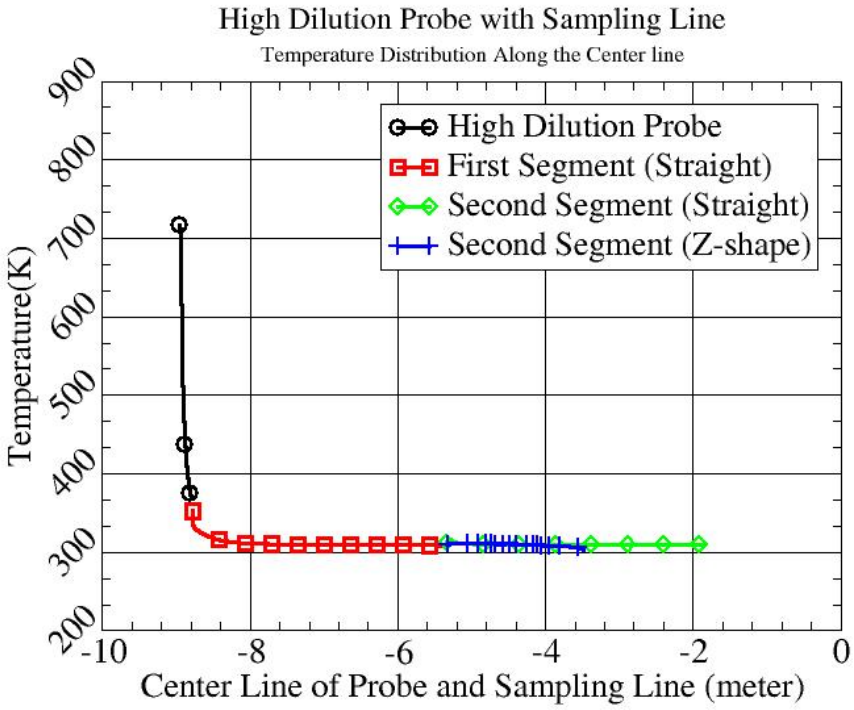

Figure 14 The temperature distribution along the center line of the probe and sampling line.

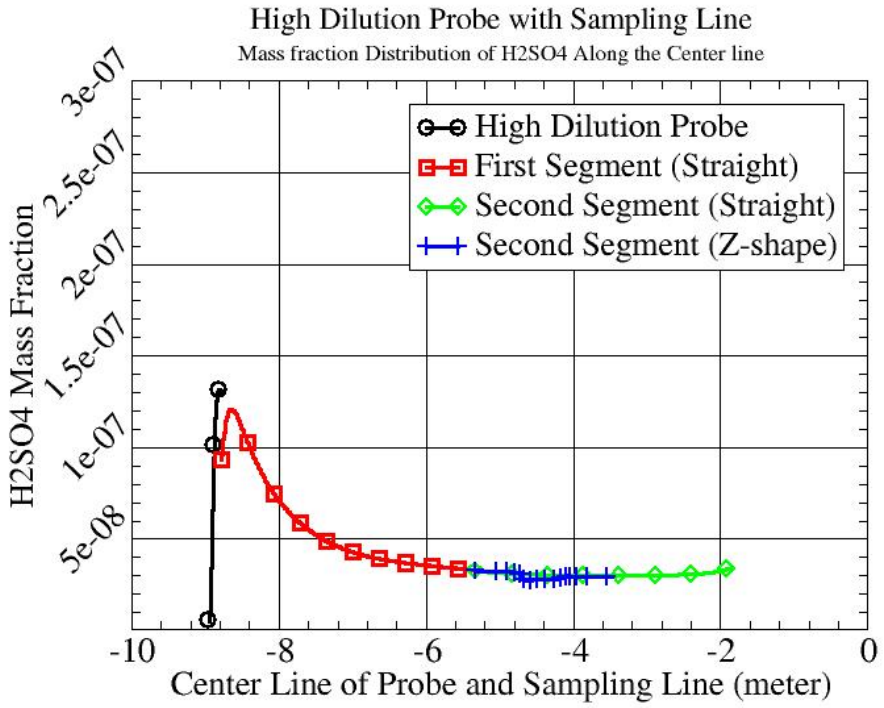

Figure 15 The gaseous H_2SO_4 distribution for the probe and sampling line.

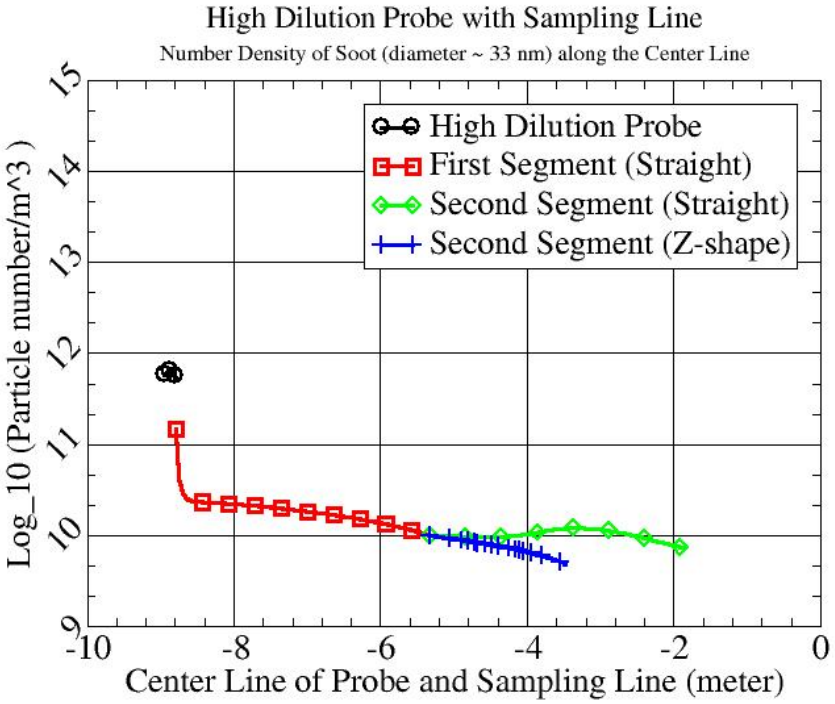

Figure 16 The number density distribution of soot particle (33 nm) for probe and sampling line.

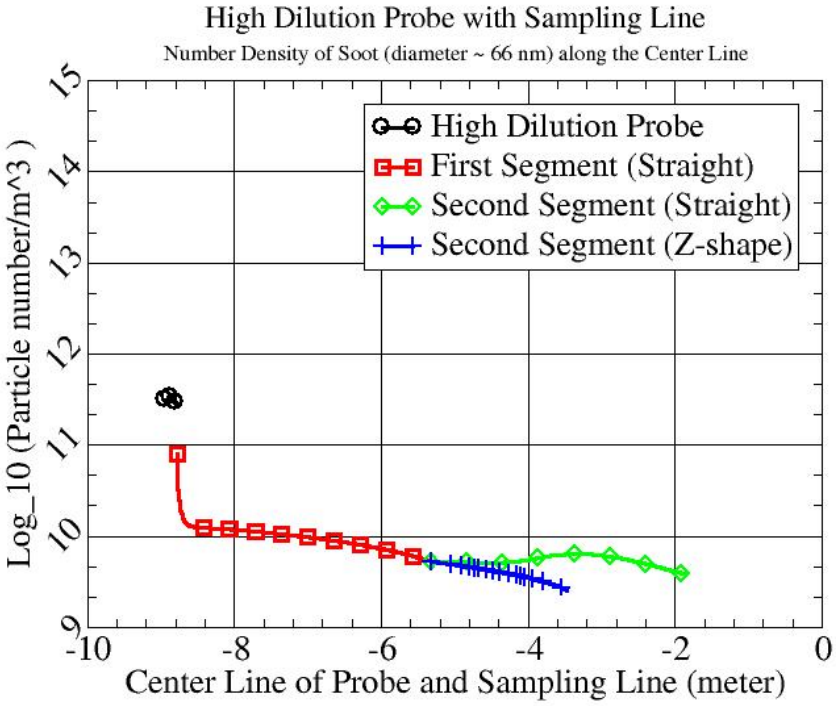

Figure 17 The number density distribution of soot particle (66 nm) for probe and sampling line.

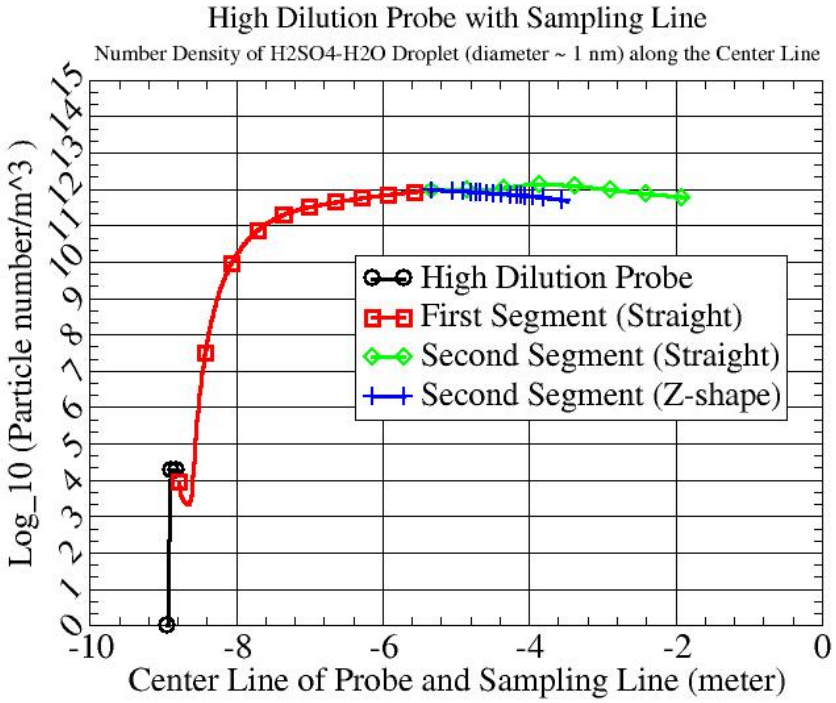

Figure 18 The number density distribution of H_2SO_4-H_2O droplet for probe and sampling line.

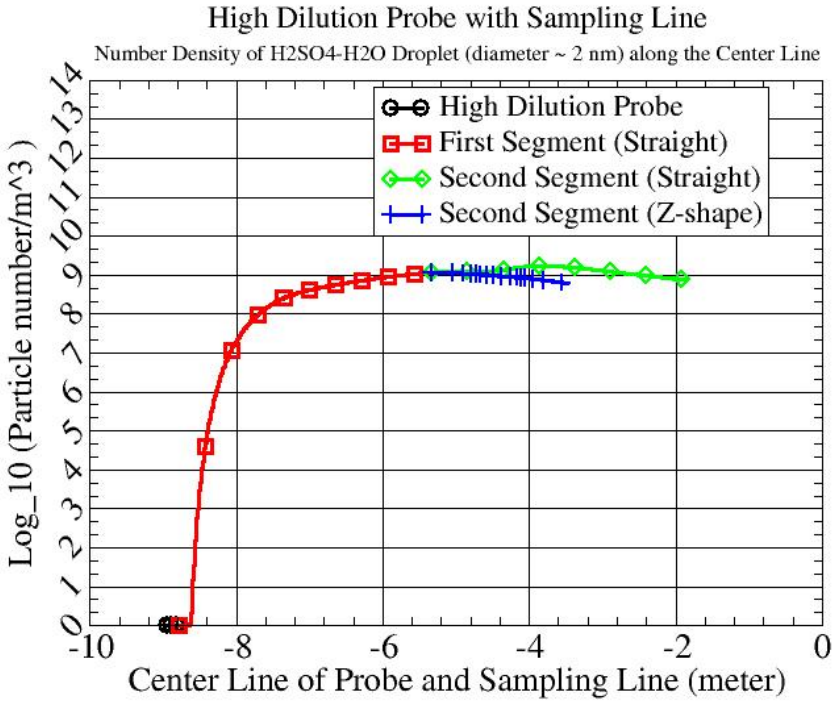

Figure 19 The evolution of H_2SO_4-H_2O droplet in probe and sampling line.

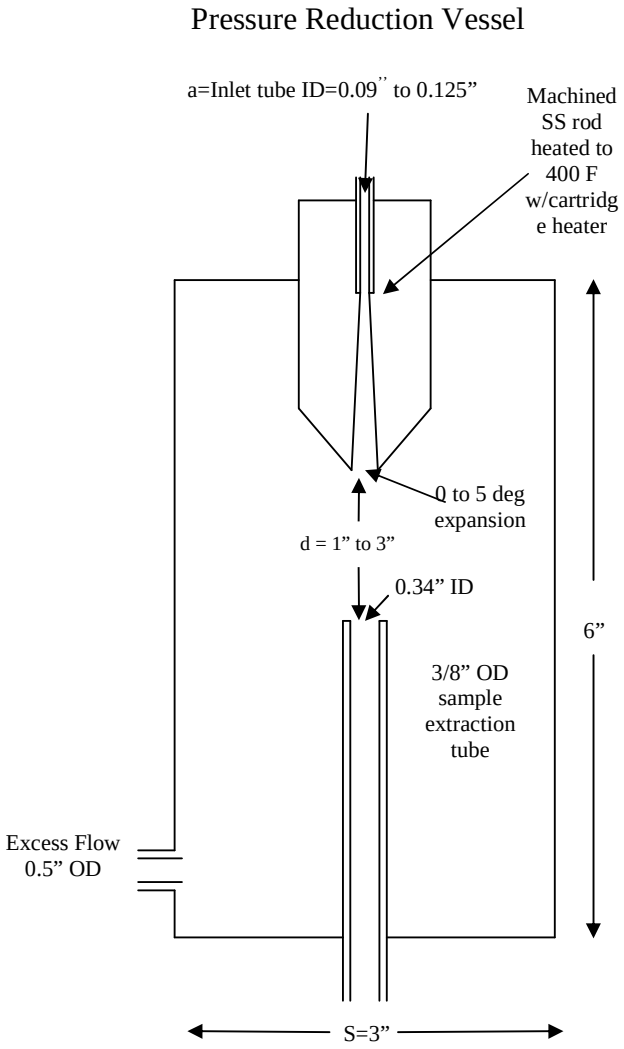

Figure 20 Schematic of a pressure reduction vessel.

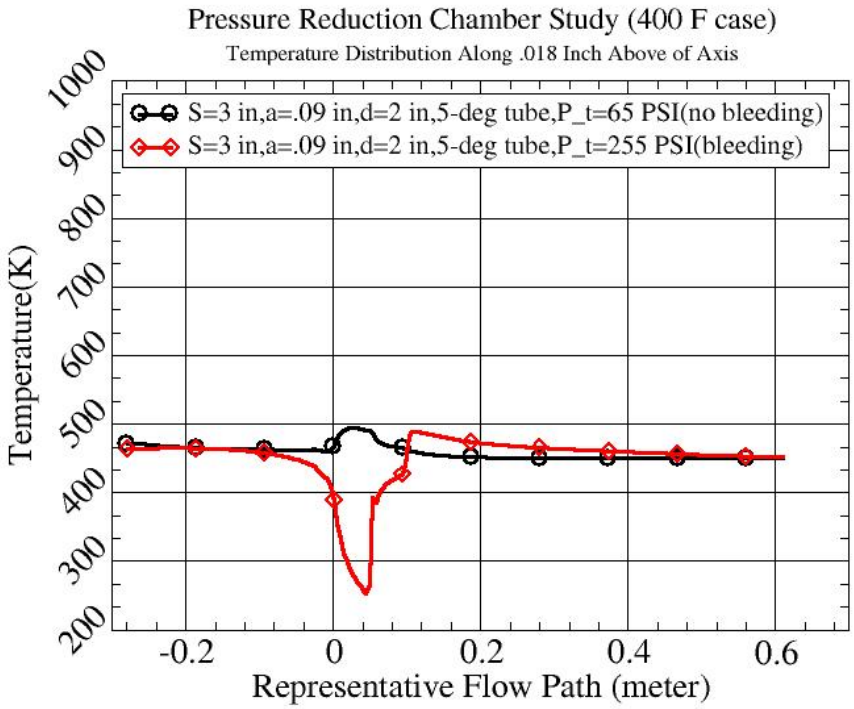

Figure 21 The temperature distribution along a line close to the center line of the device.

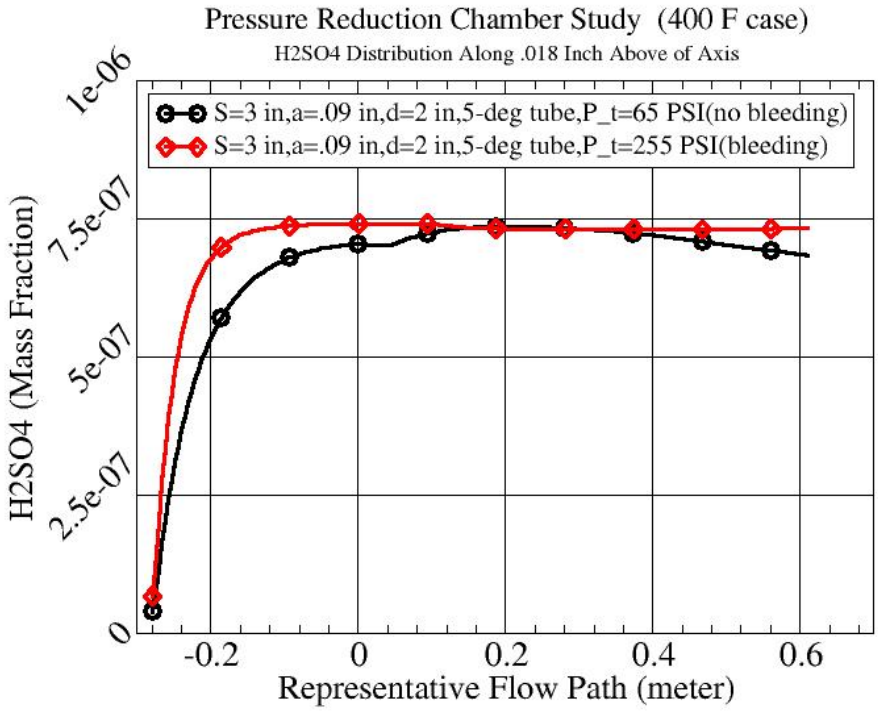

Figure 22 The H_2SO_4 distribution along a line close to the center line of the device.

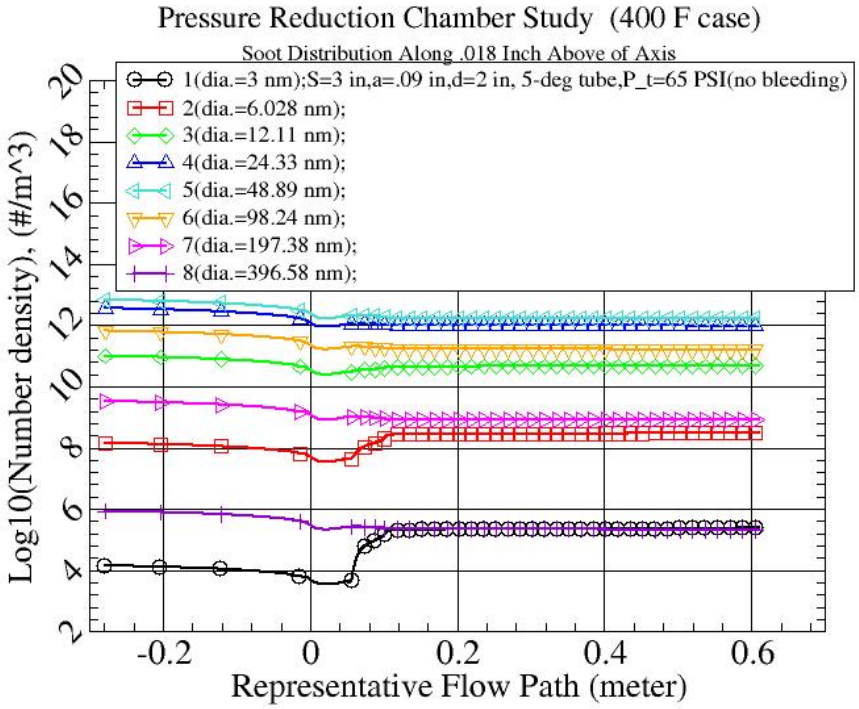

Figure 23 The number density distribution of soot particles.

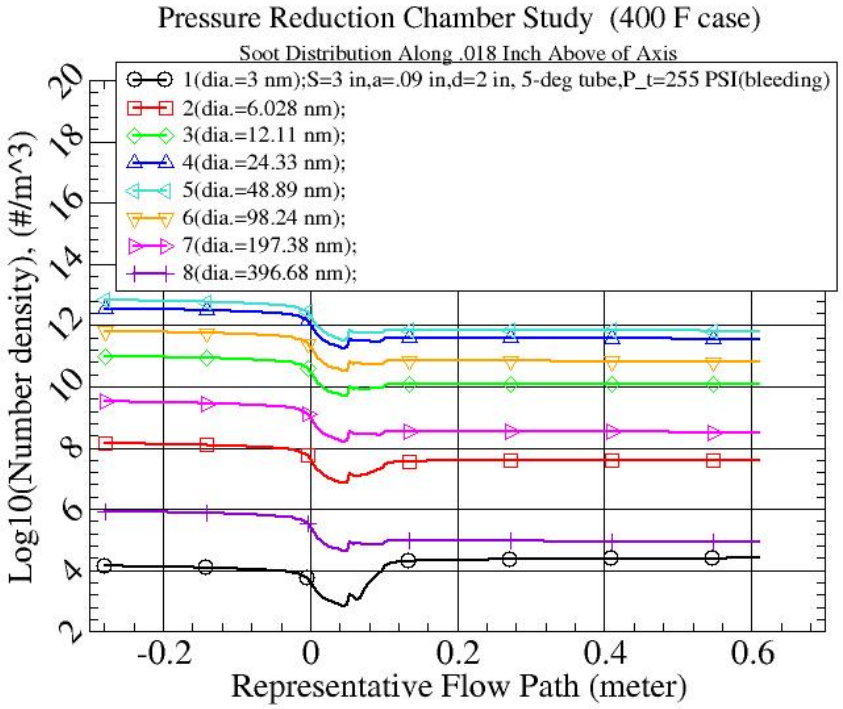

Figure 24 The number density distribution of soot particles.

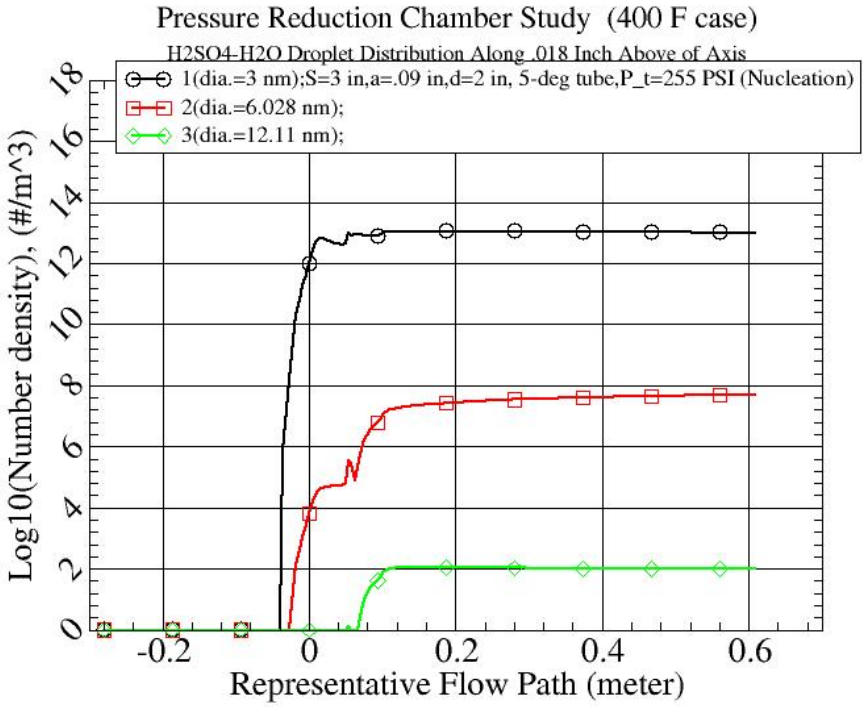

Figure 25 The number density distribution of H_2SO_4-H_2O droplets.

REPORT DOCUMENTATION PAGE

Form Approved
OMB No. 0704-0188

1. AGENCY USE ONLY (*Leave blank*)	2. REPORT DATE	3. REPORT TYPE AND DATES COVERED
	September 2006	Technical Memorandum

4. TITLE AND SUBTITLE

Modeling of Aerosols in Post-Combustor Flow Path and Sampling System

5. FUNDING NUMBERS

WBS 984754.02.07.03.06.01

6. AUTHOR(S)

Thomas Wey and Nan-Suey Liu

7. PERFORMING ORGANIZATION NAME(S) AND ADDRESS(ES)

National Aeronautics and Space Administration
John H. Glenn Research Center at Lewis Field
Cleveland, Ohio 44135–3191

8. PERFORMING ORGANIZATION REPORT NUMBER

E–15676

9. SPONSORING/MONITORING AGENCY NAME(S) AND ADDRESS(ES)

National Aeronautics and Space Administration
Washington, DC 20546–0001

10. SPONSORING/MONITORING AGENCY REPORT NUMBER

NASA TM—2006-214397

11. SUPPLEMENTARY NOTES

Thomas Wey, Taitech, Inc., Beavercreek, Ohio 45430; and Nan-Suey Liu, NASA Glenn Research Center. Responsible person, Thomas Wey, organization code RTB, 216–433–2934.

12a. DISTRIBUTION/AVAILABILITY STATEMENT

Unclassified - Unlimited
Subject Categories: 01, 02, 07, and 34

Available electronically at http://gltrs.grc.nasa.gov

This publication is available from the NASA Center for AeroSpace Information, 301–621–0390.

12b. DISTRIBUTION CODE

13. ABSTRACT ***(Maximum 200 words)***

The development and application of a multi-dimensional capability for modeling and simulation of aviation-sourced particle emissions and their precursors are elucidated. Current focus is on the role of the flow and thermal environments. The cases investigated include a film cooled turbine blade, the first-stage of a high-pressure turbine, the sampling probes, the sampling lines, and a pressure reduction chamber.

14. SUBJECT TERMS

Aeronautics; Aerodynamics; Aircraft propulsion and power; Fluid mechanics; Thermodynamics

15. NUMBER OF PAGES

59

16. PRICE CODE

17. SECURITY CLASSIFICATION OF REPORT	18. SECURITY CLASSIFICATION OF THIS PAGE	19. SECURITY CLASSIFICATION OF ABSTRACT	20. LIMITATION OF ABSTRACT
Unclassified	Unclassified	Unclassified	